THE INFLUENCES OF CARBON, NITROGEN, AND ARGON - ON ALUMINUM OXYNITRIDE SPINEL FORMATION

by

Normand Denis Corbin

B.S. Geology, Northeastern University, Boston, Mass.

(1978)

SUBMITTED TO THE DEPARTMENT OF
MATERIALS SCIENCE AND ENGINEERING
IN PARTIAL FULFILLMENT OF THE
REQUIREMENTS FOR THE DEGREE OF

MASTER OF SCIENCE

at the

MASSACHUSETTS INSTITUTE OF TECHNOLOGY

June 1982

Signature of Author _____

Department of Materials Science
and Engineering
May 7, 1982

Certified by _____

R. L. Coble
Thesis Supervisor

Accepted by _____

R. M. Pelloux
Chairman, Department Committee
on Graduate Students

THE INFLUENCES OF CARBON, NITROGEN AND ARGON ON ALUMINUM OXYNITRIDE SPINEL FORMATION

by

Normand Denis Corbin

Submitted to the Department of Materials Science and Engineering on May 7, 1982 in partial fulfillment of the requirements for the Degree of Master of Science in Materials Science and Engineering

ABSTRACT

The influences of nitrogen, argon, and carbon for producing aluminum oxy-nitride spinel (γ-ALON) were investigated using both thermodynamic and experimental data. The thermodynamic information included: free energies of reactions for producing γ-ALON, free energies of reaction for AlN and Al_2O_3 vaporization, and equilibrium vapor pressures for AlN and Al_2O_3. Experimental data obtained from powder mixture samples (Al_2O_3 + AlN, Al_2O_3 + C, Al_2O_3 + Al) and pure components included weight losses, microstructural development, and percent of γ-ALON formed.

Below ~1625°C sintering occurred without densification, and no γ-ALON formation was observed. Argon gas promotes larger weight losses than nitrogen while no carbon effects were observed. It appears that the nitrogen atmosphere suppresses the AlN decomposition.

Above ~1625°C γ-ALON forms, and densification occurs. Argon gas produces larger weight losses and coarser microstructures than does nitrogen. Both carbon and aluminum vapor (from AlN decomposition) facilitate the formation of γ-ALON from αAl_2O_3.

It appears the development of vapor species strongly influences weight losses, sintering, and γ-ALON formation. The presence of these species can be modified by changing the atmosphere in the furnace.

Thesis Supervisor: Dr. Robert L. Coble

Title: Professor of Ceramics

TABLE OF CONTENTS

TABLE OF CONTENTS (Cont'd)

TABLE OF CONTENTS (Cont'd)

LIST OF FIGURES

LIST OF FIGURES (Cont'd)

LIST OF TABLES

Acknowledgements

Of all the people who assisted me during my research and studies at MIT, the most influential was my wife Linda. Her encouragement, understanding, and love gave me the support I needed during my studies there.

I thank Prof. Robert Coble for his advice, guidance, and interest in my research project.

I also thank my office mates whose friendship made my brief stay at MIT a very memorable and enjoyable one. To Hanill for the discussions of Korea and thermodynamics, to Alexana for her smile and interesting conversation, to Elaine for being my thesis editor and hockey teammate, and to Elena who shared the drudgery of thesis writing with me.

Finally, I thank Dr. James McCauley and Dr. Robert Katz at AMMRC, who encouraged me to continue my education and assisted me in obtaining approval to attend MIT on a full time basis. I also thank Ms Louise Teti at AMMRC for her valuable technical assistance, and Mrs. Barbara Marks for the typing of my thesis.

I. Introduction

Aluminum oxy-nitrude spinel (γ-ALON) is a relatively new ceramic material which may have distinct advantages over sintered polycrystalline α-Al_2O_3. Alpha-alumina is an anisotropic material. As a result, true optical transparency of polycrystalline Al_2O_3 is impossible. Further, significant strain can result at grain boundaries due to thermal expansion mismatch of individual grains. An approach to solving this anisotropic problem is the stabilization of a cubic form of Al_2O_3 by the addition of AlN. This spinel material, aluminum oxy-nitride (γ-ALON), has been fabricated into fully dense and transparent polycrystalline bodies.

Presently the only fundamental evaluations on this material include a crystal structure analysis (22) and grain growth data (18). Little is understood about the reaction mechanism for producing γ-ALON from αAl_2O_3 other than temperatures above 1600°C are required. This study will evaluate thermodynamic and experimental data on γ-ALON reactions to better understand the reaction mechanism.

II. Literature Review

II.1 γ-ALON History

Aluminum oxide is known to exist in many different crystalline forms below 1100°C(1). One of these is a spinel type (2) (γ-Al_2O_3), but it converts to the corrundum structure (α-Al_2O_3) above ~ 1000°C. Aluminum oxide's high strength, chemical resistance, and electrical insulating properties make it a very important ceramic material; however, because the stable high temperature form is noncubic, it has significant directional variations in its properties. The variation of its refractive index with direction makes it impossible to obtain true optical transparency of polycrystalline α-Al_2O_3. If Al_2O_3 could be stabilized into a cubic structure, this transparency problem would be eliminated. Also it would improve the thermal expansion mismatch which can produce significant stress in polycrystalline α-Al_2O_3 bodies (3).

It has been known since 1946 (4) that a spinel form of Al_2O_3 can be stabilized at high temperature (> 1100°C). The initial investigators (4-8) believed the spinel phase formed by reduction of the Al^{+3} to Al^{+2}; this would be identical to the reduction of Fe^{+3} to Fe^{+2} to form Fe_3O_4 spinel. In 1959 Yamaguchi (9) published results which determined the spinel phase was stabilized not by Al^{+2} but by nitrogen. Since his work several investigations into forming this spinel, hence forth referred to as γ-ALON (gamma Aluminum oxy-nitride) have been conducted.

Currently, studies on aluminum oxy-nitride materials are associated with three areas of technology:

(a) Aluminum Nitride (AℓN) is currently under investigation and it is known that by using Al_2O_3 as an additive, the sintering characteristics are greatly improved (10,11, 12,13),

(b) Silicon Aluminum Oxynitride (MSiALON) related materials, where M = Metallic ion, are being investigated (14,15, 16) and the understanding of phase relationships in these quinary systems is aided by an accurate AℓN-Al_2O_3 binary phase diagram, and

(c) γ-ALON is becoming of interest in itself since the properties currently evaluated project it as being an important cubic, transparent, strong, and chemically resistant refractory material.(17,18)

II.2 AℓN-Al_2O_3 Phase Relationships

In order to fabricate single phase γ-ALON it is important to understand the phase relationships in the Al-O-N ternary phase diagram. Presently all studies in this ternary have been conducted along the pseudo-binary between AℓN and Al_2O_3. Current experimental information on the phases in this binary shows that as many as thirteen different phases can occur. Five of these phases have only been documented by one investigator leaving eight which are verified. Table 1 lists all thirteen phases along with their nomenclature, approximate composition, and investigators.(16,19-31).

The commonly called "Aluminum Nitride Polytypes" are phases based on the AlN structure found in the Si-Al-O-N system (15). These phases appear compositionally controlled and therefore not true polytypes (ex. SiC). Similar structures can be stabilized without silicon, as shown by AlN-Al_2O_3 studies. The compositions of these phases (Table 2) were calculated using the information that they are stable at specific metal to nonmetal ratios (19,14) and allowing for change neutrality.

The composition of the spinel phases γ-AlON and Ø'-AlON were taken from the model calculations of McCauley (24). Phase γ'-AlON Spinel was found upon oxidation of γ-AlON by Goursat (25,26). Phase Ø-AlON was determined by Michel (27) to be monoclinic and occur upon oxidation of δ-ALON which in his work had a composition containing more nitrogen than Ø-ALON. The δ-ALON phase was observed by many investigators, with its composition ranging from 12 to 4 mole % AlN depending on the author.

The first phase diagram for this system was determined by A.M. Lejus (28) (Fig. 1). Six phases were identified with the phase designated as (X) encompassing the AlN-polytype phases. This diagram does not show high temperature stability limits for either the (X) or γ-ALON phases, but does give the first detailed information of the γ-ALON solid solution composition range. Her data shows γ-ALON solid solution centered around the $25^m/o$ ALN composition and does not include the ideal spinel composition at $50^m/o$ AlN or Al_3O_3N

(3 cation 4 anion, ex. $MgAl_2O_4$).

Since Lejus' early work the diagram has been modified by Gauckler (16), Sakai (11) and McCauley and Corbin (29,30). All of the diagrams generally agree, with each newer version becoming more complex while improving the preceding work.

The most recent work was conducted by McCauley and Corbin. Their earliest diagram has γ-ALON incongruently melting at ~ 2050°C and they also observed the same relationship between the polytypes like phases and temperatures as reported by Sakai. Their results differ remarkably from Lejus as to the exact position of the γ-ALON solid solution field. Lejus had it centered at $25^m/o$ AℓN while this work uses $35.7^m/o$ AℓN, and shows a deep eutectic which forms near $25^m/o$ AℓN. In the latest work (Fig. 2) a complete diagram for this pseudo binary was attempted including liquid and vapor species. This work has γ-ALON melting congruently at 2165°C which was determined using single phase γ-ALON samples and temperatures calibrated with the melting points of α-Al_2O_3 and $MgAl_2O_4$ samples. This study did not investigate regions where δ-ALON is stable, hence it is not entered on the diagram. Other investigators studied phases in this system, several are listed in Table 1.

The AℓN-Al_2O_3 phase equilibrium diagram has also been calculated using thermodynamic data. Both Dorner (32-33) and Kaufman (34) assumed the $25^m/o$ AℓN (AL_7O_9N) composition for γ-ALON. Their calculations resulted with this phase being the only thermodynamically stable phase in the system. The

results of their works differ considerably as to the stability of γ-ALON and its melting characteristics. Dormer has this phase incongruently melting at 2000°C and only stable above 1600°C while Kaufman has γ-ALON congruently melting at ~1940°C and stable at room temperatures. From the recent work of McCauley and Corbin and information in this thesis, Kaufman's relationships are more representative of γ-ALON, but his melting point is at least 200°C too low. Their calculations and assumptions will be further discussed in the thermodynamic discussion of this thesis.

II.3 γ-ALON Composition

The limits of solid solution for γ-ALON have yet to be carefully characterized. The major reason for the differences between the work of various investigators, as shown in Table 3, is few samples have been analyzed for aluminum, oxygen, and nitrogen concentrations after fabrication. These results should be in better agreement if this kind of analysis was conducted. A major finding in agreement with everyone is the solid solubility region is not centered at the ideal spinel composition of Al_3O_3N (50^m/o AlN) but is more oxygen rich. The range of solid solubility is generally between 50^m/o AlN and 25^m/o AlN. Table 3 also shows three general spinel formulas which have been used to model the spinel region from Al_3O_3N to Al_2O_3, which may also have a spinel structure. All models make the assumption of a constant anion lattice where nitrogen is substituted for oxygen. In

these formulas as the nitrogen content increases the spinel cation vacancies decrease until at the composition Al_3O_3N no vacancies remain.

II.4 γ-ALON Crystal Structure

From the very early result of Yamaguchi, it was known that a high temperature spinel form of Al_2O_3 could be stabilized with nitrogen. On the atomic scale, this stabilization results in destabilizing the Al_2O_3 corrundum structure in favor of a spinel structure by substituting nitrogen for oxygen in the lattice. This rearrangement involves reorganizing the oxygen anion hexagonal close packed structure to an oxygen plus nitrogen cubic close packed structure, while shifting the aluminum cations from all being in octahedral positions to one third now being in tetrahedral positions.

Recently, Goursat et al (22) have determined the crystal structure of γ-ALON using neutron diffraction data; this work confirms the structure as a (Fd3m) spinel. They confirmed that oxygen and nitrogen occupy the anion sites with aluminum cations occupying the tetrahedral and octahedral sites of the spinel structure. The stability of this spinel phase was found to occur only when there is a disordered vacancy in the spinel octahedral positions. Unlike many spinels, γ-ALON solid solution does not include the classical spinel AB_2X_4 composition Al_3O_3N.

Since a trivalent ion (Al^{+3}) is in the tetragonal position, this structure can be thought of as an inverse

spinel structure. Table four compares stochiometric spinels (normal and inverse) (35) to nonstochiometric oxynitride compositions (24,26) and γ-alumina (24). To construct this table all the spinel anion sites and all the spinel tetragonal sites are assumed filled. In these oxynitride phases there are no divalent ions available to enter the octahedral positions as in a true inverse spinel. The excess charges due to trivalent aluminum in a divalent position are stabilized by the simultaneous substitution of trivalent nitrogen for divalent oxygen in the anion position .

Lattice parameter data for the solid solution region is plotted in Fig. 3. Lejus and McCauley data have similar results but there is roughly a five mole % AℓN disagreement between their lattice parameter values. This can be attributed to both investigators plotting prefired compositions data and not the composition of as fired samples. This difference could also be due to the processing methods used, oxidation levels in the starting AℓN powders, or different firing times. Because Lejus had determined a larger γ-ALON solid solubility region her lattice parameters have a larger range in values (Fig. 1).

II.5 γ-ALON Fabrication

In the literature there are several methods used for obtaining various aluminum oxynitride phases. The known reactions fall into three categories: (1) using alumina, (2) using aluminum, and (3) gas phase reactions. Table 5

lists the basic, unbalanced, reaction equations which produce either single phase γ-ALON or a mixture of γ-ALON and other aluminum oxynitride phases.

A common method for γ-ALON fabrication involves mixing Al_2O_3 and AlN powder in the proper proportions (equation 1), then reacting at temperatures above 1700°C. Depending on the interest of the investigator the procedure can be modified to produce either powders (18,25,26), reaction-sintered samples (17,29), or reaction-sintered hot-pressed material (19,31,36). A major problem with the above method is the requirement to use AlN powder for fabrication. As previously discussed (37) the characteristics of the AlN powder (including lot consistency, impurities, unreacted components, and particle size distribution) are critical for producing dense material. If high purity AlN must be purchased, the cost for producing γ-ALON could become prohibitive. Therefore, other methods for producing this material without the use of AlN may be important in the future.

Other fabrication methods include simultaneous reduction and nitridation of Al_2O_3 powder. The benefit in these processes is using Al_2O_3 powder which can be obtained at high purity and controlled physical characteristics at reasonable cost. Table 5 equations 2a to 2e show how Al_2O_3 can be reduced with aluminum, carbon, or ammonia. Collongues (42) reported "Nitrogen is inert with respect to Al_2O_3 except in the presence of reducing agents." It is this capability which allows

γ-ALON formation from Al_2O_3. Rafaniello (38) and Ish-Shalom (39) have formed powders by heating mixtures of Al_2O_3 with carbon (16:1 by wt.) at 1700°C in a nitrogen atmosphere. Similar work was done in the 1950's (7,8,9) when alumina and graphite mixtures were heated at 1700°C in a Tammann furnace with air. Many people have used this kind of nitridation/ reduction of alumina to produce AlN powder by simply increasing the amount of carbon in the mixture to remove all oxygen. Work by Michel et al (40) and Collongues (41) have observed various Al-oxynitrides when melting Al_2O_3-Al mixtures in air. They did not produce single phase material but mixtures of γ-ALON and δ-ALON resulted. Studies concerning the stability of Al_2O_3 in ammonia were done by Collongues (42,43). This work found that above 1000°C ammonia can react with Al_2O_3 to form AlN in the presence of hydrogen. When this reaction is done above 1650°C the phases γ-ALON and δ-ALON will form.

Aluminum oxynitrides can also be formed from aluminum metal (Table 5, Eq. 3) as observed by Michel (44) and Bouriannes (45,46). Michel noted that at high temperatures, aluminum liquid can react with air to form various aluminum oxynitrides. Bouriannes, conducted studies of the combustion of aluminum spheres (~3mm dia.) in various atmospheres. By rapidly induction heating his samples in air, until combustion occurred, he could form γ-ALON. These results depend strongly on the gas pressures used ($p > 70$ bar = γ-ALON, $p < 70$ bar = αAl_2O_3). Once the combustion reaction was

initiated (about 1500°C), the samples rapidly heated to ~2200°C due to the exothermic combustion reaction.

Various aluminum oxynitride compositions have been successfully deposited by chemical vapor deposition techniques (47-52). Irene (47) and Silvestri (48) were able to use reaction 4 in Table 5 to produce thin polycrystalline spinel layers on silicon substrates, at 900°C the γ-ALON phase was observed while at 770°C the zeta-Al_2O_3 (zeta-ALON) phase was observed. They were able to fabricate different compositions in the ALN-Al_2O_3 pseudo-binary by changing the NH_3/CO_2 ratio. It is important to note this work uses the lowest reaction temperatures recorded to produce γ-ALON. A very similar reaction mechanism was recently used (49,50) to surface treat highspeed cutting tools with various aluminum oxynitride compositions.

As can be seen, a variety of processing routes can be used to fabricate γ-ALON. The reason for generally using high temperatures (>1600°C) to produce this material may be a result of using Al_2O_3 powders, especially since much lower temperatures are used for gas reactions. This would also account for the high temperatures required when aluminum is used, since an oxide surface layer is always present (53). This information along with a thermodynamic evaluation of γ-ALON formation will be discussed in a separate section of this thesis.

II.6 γ-ALON Properties

Currently, it appears many property evaluations of

γ-ALON may be largely effected by extrinsic influences including porosity, secondary crystalline phases, glassy phases, and impurities. In this property review, the occurence of these extrinsic variables will be highlighted when they appear to be important.

Several investigators have reported properties for γ-ALON including polycrystalline sintered bodies (11,13,17,18) powders (6,25,26), and γ-ALON plus other Aℓ-oxynitride hot pressed composites(31,36). Since this review is interested in primarily single phase γ-ALON the hot pressed composites will not be discussed. Table 6 summarizes the reported property data on polycrystalline γ-ALON.

II.6.1 Optical and Dielectric

Since γ-ALON is being considered as an electromagnetic window material, various optical and dielectric property evaluations have been conducted. The in-line transmission spectra show this material as having an infra-red cutoff at 5.2μm (50% transmission) and an ultra violet cutoff near .3μm (17,18). Samples sintered to greater than 99% theoretical density by Hartnett et al (18) show window glass clear transparency in the visible region of the spectrum. Refractive indices for the spinel solid solution varies from 1.770 (30^{m}/o AℓN) to 1.875 (37.5^{m}/o AℓN) (8,9,17) using λ = .55μm.

Variations in the dielectric constant and dielectric loss tangent as functions of frequency and temperatures are

shown in Figs. 4 and 5. Both of these properties increase in value as the temperature increases and/or frequency decreases. These relationships are expected for both intrinsic and extrinsic effects (54). For a pure single crystal, the same relationships as shown for the dielectric properties of γ-ALON occur due to the combination of intrinsic limitations including ion mobility, crystal imperfection mobility and dc conductivity effects. Similar relationships observed for the loss tangent can be explained due to ion migration losses and impurities. For polycrystalline and poly-phase ceramics, these same relationships can be explained by extrinsic limitations such as grain boundaries, porosity, and electronic-ionic interactions between the various phases. When glassy phases occur, they are known to be a major contributer to dielectric losses and therefore their compositions are critical. Upon close evaluation and characterization of the tested γ-ALON samples, it was found to contain both porosity (~2%) and a glassy grain boundary phase which contains impurities derived from AlN percursor powder (55). With this knowledge, it appears these results could be improved especially at low frequencies and high temperatures by producing theoretically dense, single phase, high purity samples.

The magnetic susceptability was evaluated to be (-0.34×10^{-6}/g) using the Gouy method with an applied field of 13000 gauss (9).

II.6.2 Mechanical

Little work has been done on characterizing the

mechanical properties of polycrystalline single phase γ-ALON. Recently Corbin and McCauley (17) have evaluated some of the properties which are summarized in Table 6.

Microhardness values of 1650-1800 $^{Kg}/_{mm^2}$ were obtained on individual γ-ALON grains in a dense polycrystalline body using knoop indentation with a 100g load. The elastic modulus and Poisson's ratio range from 47.3 x 10^6 to 46.7 x 10^6 psi and .249 to .263, respectively, as determined by ultrasonic methods. Four point fracture strengths range from 44.4 x 10^3 psi at room temperature to 38.7 x 10^3 psi at 1000°C.

The above properties were all evaluated on coarse grained (25 μm and 100 μm) samples which contain some traces of secondary phases. The authors believe future improvements in processing will reduce secondary phases and grain size, thus improving the mechanical properties.

II.6.3 Thermal Properties

Thermal properties were evaluated by Sakai (11,56) on hot pressed γ-ALON samples and Corbin and McCauley (17) on sintered samples. Table 6 also summarizes these properties. The thermal expansion coefficient varies from 5.23 x 10^{-6}/°C (25°C to 200°C) to 7.0 x 10^{-6} (20°C to 980°C) for reaction-sintered material while for hot pressed samples it is 7.59 x 10^6/°C (25°C to 1000°C). The values for room temperature thermal conductivity, thermal diffusivity and specific heat as determined by Sakai are listed in Table 6.

The water quench thermal shock resistance for sintered

γ-ALON is shown in Fig. 6 with a ΔTc of 175 ± 5°C, this value is somewhat lower than αAl_2O_3 (ΔTc = 210°C, AD-99) (17). It is believed the thermal shock resistance of γ-ALON should be comparable to αAl_2O_3 since less grain boundry stress will result while quenching a cubic material and it has a smaller thermal expansion. The current lower value may be due to the presence of minor secondary phases, differences in thermal conductivities (γ-ALON/αAl_2O_3 = 1/3), and/or problems in fabricating large samples.

II.6.4 Oxidation and Chemical Resistance

There is disagreement on the stability of γ-ALON in an oxidizing environment. Corbin and McCauley (17) testing bulk samples in air found the oxidation to form a protective oxide layer up to ~1200°C. Billy (57) found the oxidation of γ-ALON powders to start at ~650°C in oxygen (p = 32 torr) and not form a protective layer.

Recent work by Goursat (25,26) investigates the oxidation kinetics of γ-ALON and the formation of another phase (γ'-ALON) during the oxidation process. Figure 7 taken from his work is a thermal gravemetric analysis (TGA) trace showing the oxidation behavior of 20-50 μm powder. As shown, oxidation starts near 650°C, then rapidly increases above 800°C to a maximum near 1150°C (~7.2% wt. gain). Further heating above this temperature produces a reduction in the percent weight gained for the sample (~4.5%). The maximum is attributed to γ-ALON oxidizing without nitrogen loss

which forms a new phase (γ'-ALON, also a spinel) with a composition near $Al_{2.46}\boxed{s}_{.54}(ON)_4$. Heating to temperatures above this maximum results in oxidation with nitrogen loss to form αAl_2O_3. Complete oxidation from γ-ALON to αAl_2O_3 corresponds to the reaction equation:

$$4\ Al_{23}O_{27}N_{5(\pm s)}\ 15\ O_{2(g)} \rightarrow\ 46Al_2O_{3(\pm s)}\ 10N_{2(g)}\ (+4.2\%wt.\Delta)$$

Goursat et al also studied the oxidation kinetics to form γ'-ALON from γ-ALON at 32 torr oxygen. It appears two kinetic regimes for this oxidation can exist: a reaction controlled, and a diffusion controlled. The regime which results dependson the powders physical characteristics. The formation of γ'-ALON as an intermediate oxidation phase depends on the actual composition of the γ-ALON material. At γ-ALON compositions high in nitrogen content the intermediate step is not seen and oxidation proceeds directly to αAl_2O_3. This phenomenon is not yet understood.

Resistance of this material to other forms of chemical attack has been investigated (7,8,9,58) with the results showing γ-ALON resistant to acids, bases, and H_2O.

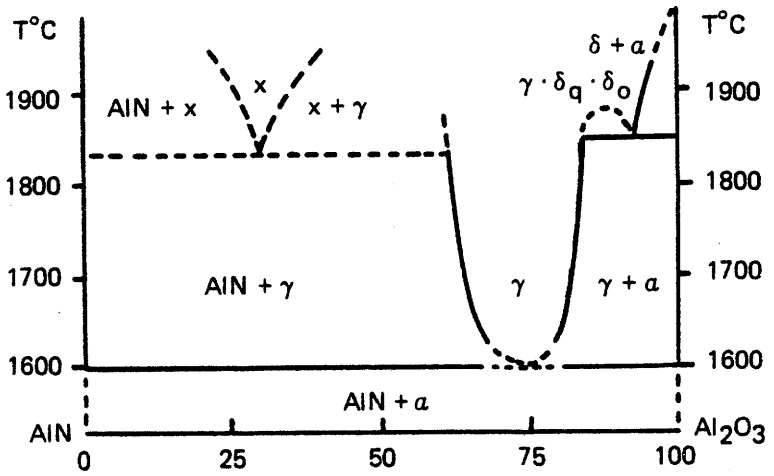

Figure 1. PHASE DIAGRAM FOR THE Al_2O_3-AlN SYSTEM (Lejus 1964)

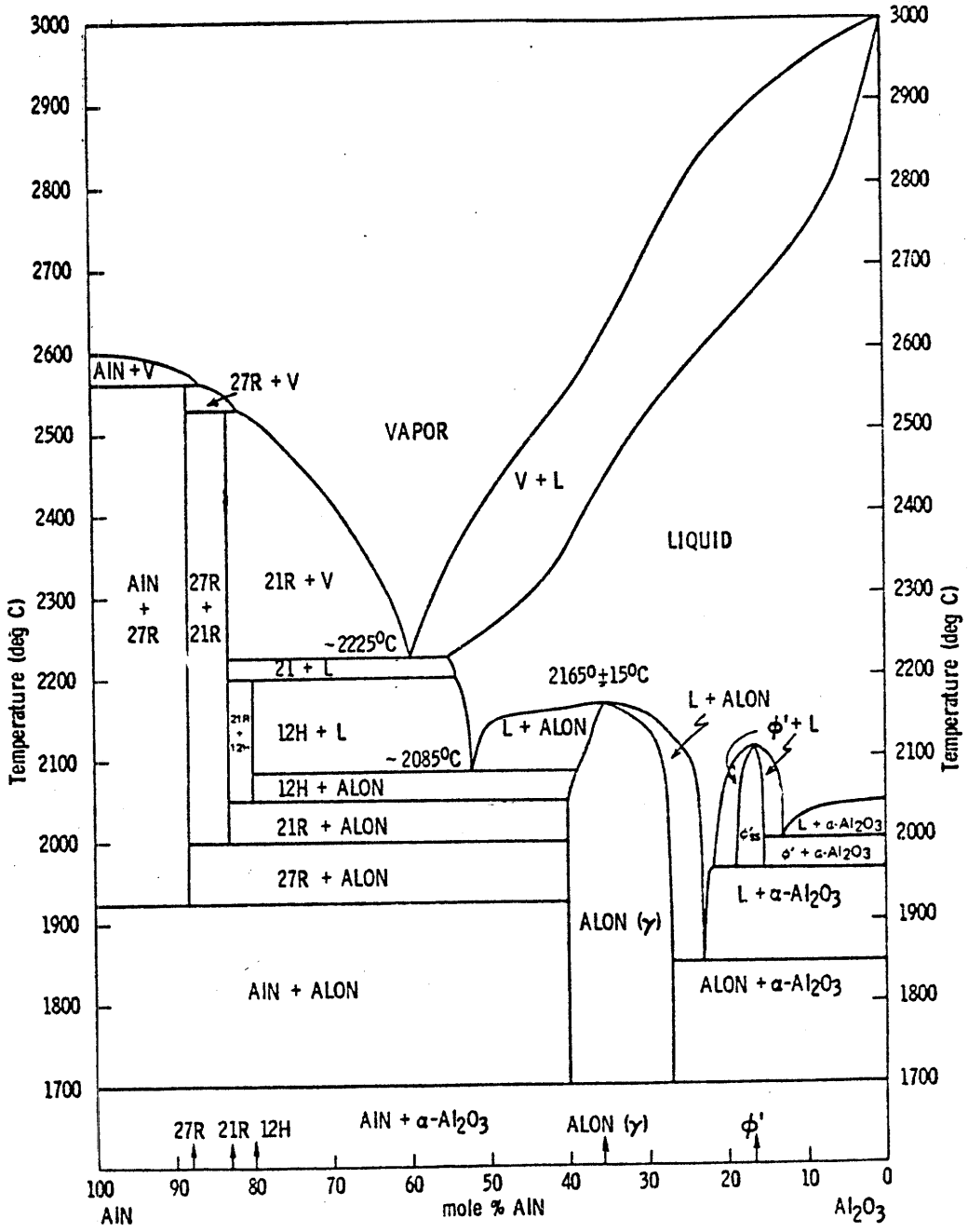

Figure 2. PHASE DIAGRAM FOR THE Al_2O_3-AlN PSEUDO-BINARY (McCauley-1981)

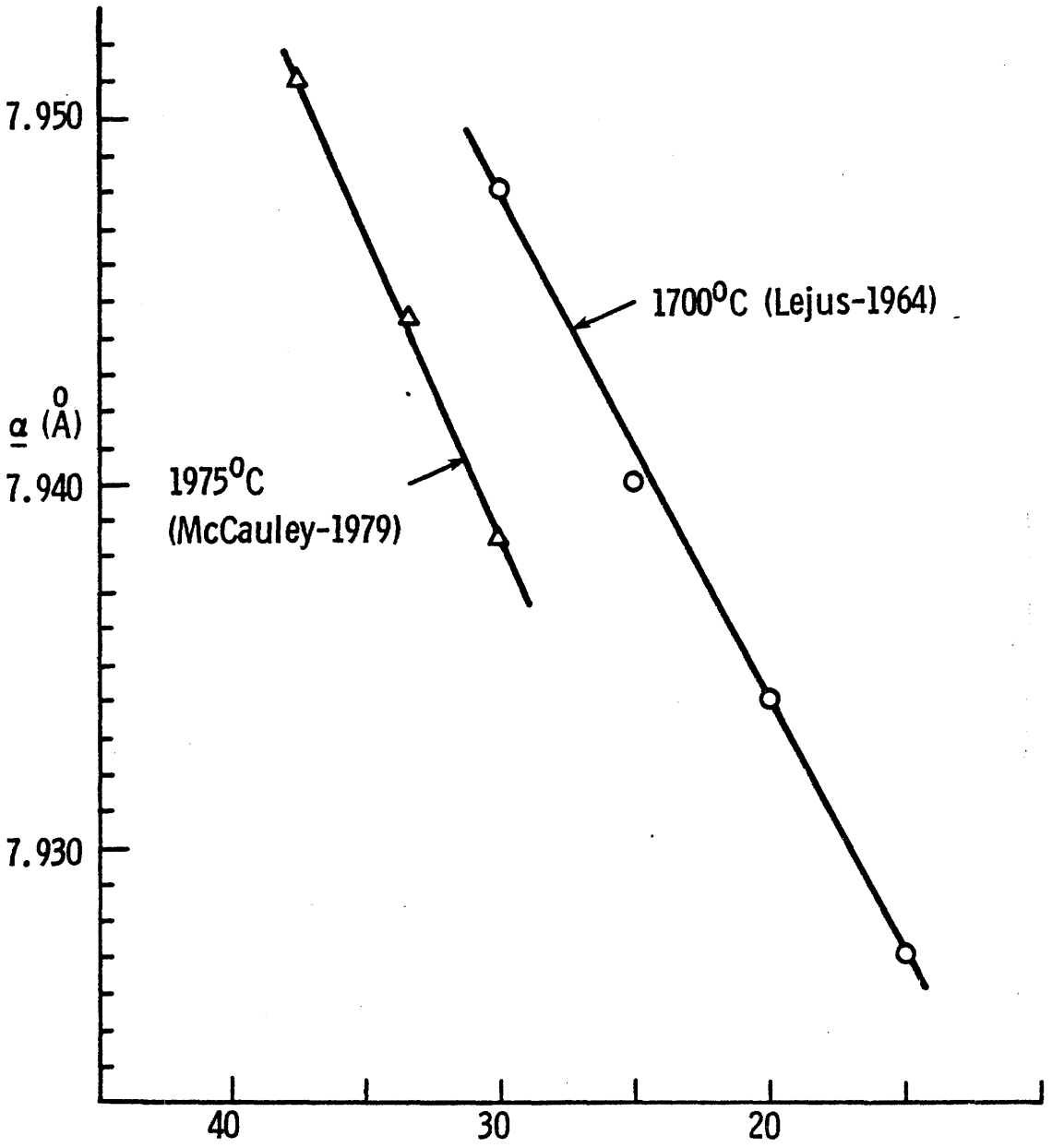

Figure 3. LATTICE PARAMETERS OF γ-ALON AS A FUNCTION OF MOLE % AlN

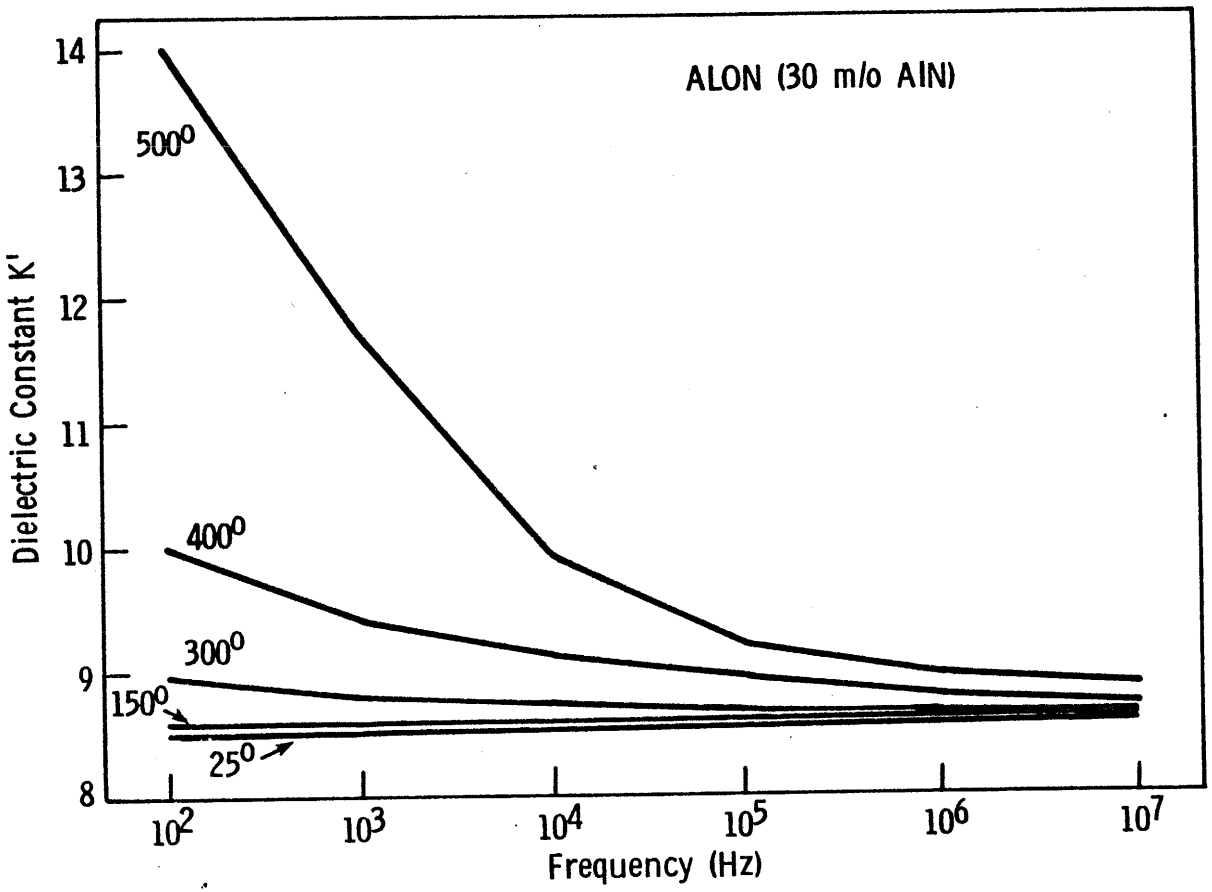

Figure 4. DIELECTRIC CONSTANT VERSUS FREQUENCY (Corbin-1981)

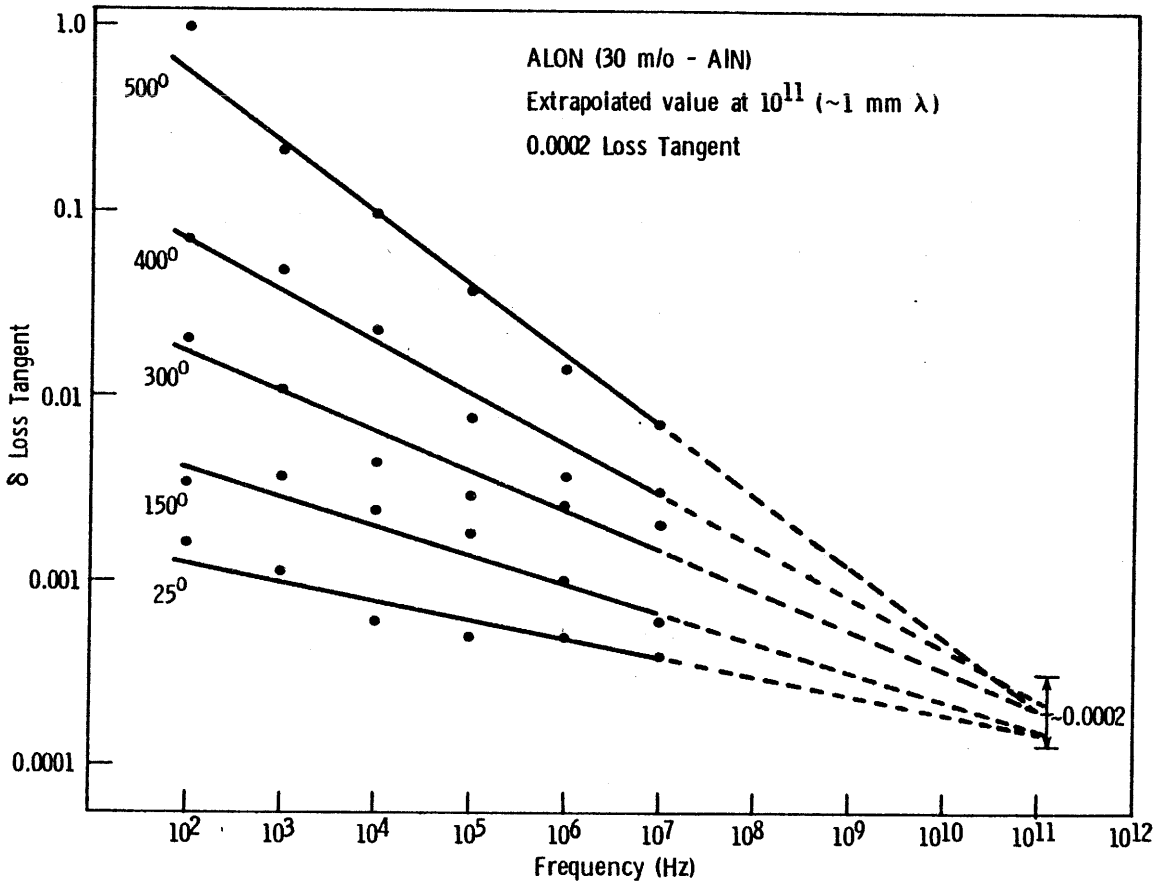

Figure 5. LOSS TANGENT VERSUS FREQUENCY (Corbin-1981)

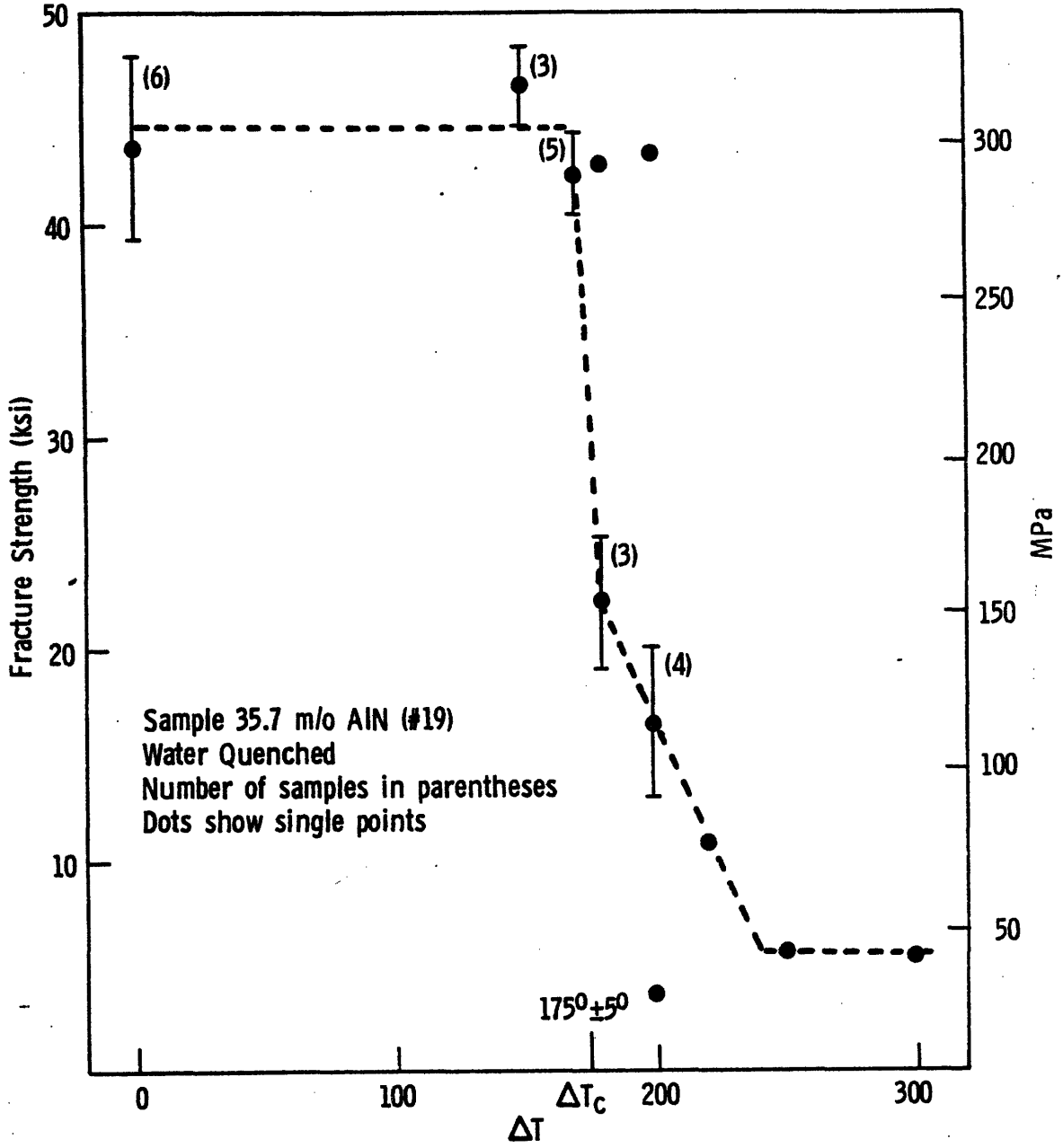

Figure 6. ALON THERMAL SHOCK RESISTANCE (Corbin-1981)

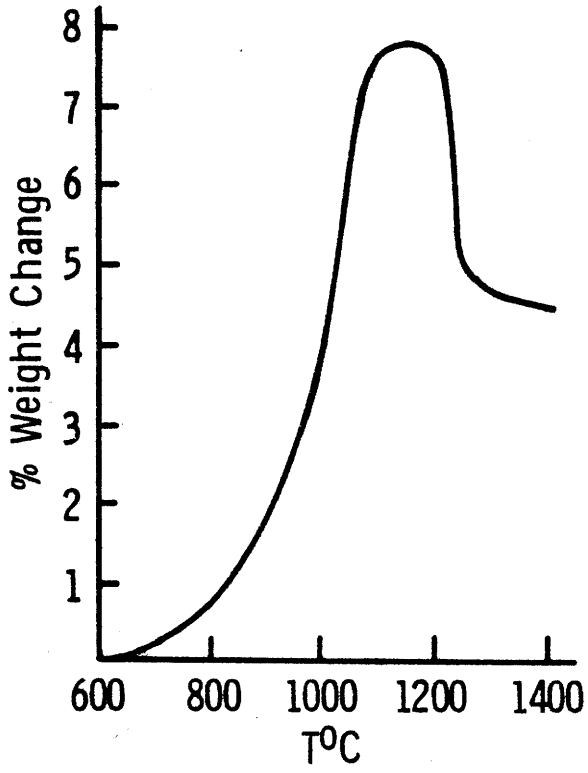

Figure 7. THERMOGRAVAMETRIC ANALYSIS (TGA) OF γ-ALON IN OXYGEN (32 torr) (Goursat 1976)

Table 1. ALUMINUM OXYNITRIDE PHASES

	AlN	Polytypes of AlN						Spinel					
	2H	$2H^{\delta}$	20-H	27-R	16-H	21-R	12-H	γ	γ'	ϕ'	ϕ	δ	Al_2O_3
Mole % AlN	100	-	88.9	87.5	85.7	83.3	80.0	35.7	~21.0	16.7	7.1	4-10	0
References													
Adams (1962)	X	←					→	X				X	X
Lejus (1964)	X	←					→	X				X	X
Long (1961)	X									11.4		X	X
Henry (1969)	X	←					→	X		←		→	X
Michel (1972)								X		X	X	X	
Gauckler (1976)	X			X		X		X				X	X
Sakai (1978)	X	X		X	X	X	X	X					
McCauley (1981)	X			X		X	X	X		X			X
Goursat (1981)								X	X				X
Bartram (1979)	X		X	X									

←→ Identified Phase

Table 2. AlN "POLYTYPE PHASES"

Ramsdell Phase Notation	M : X	Formula	Mole % AlN
2-H	1 : 1	AlN	100
20-H*	10 : 11	$Al_{10}O_3N_8$	88.9
2-H$^{\delta t}$	>9 : 10	-	>87.5
27-R	9 : 10	$Al_9O_3N_7$	87.5
16-H^{t}	8 : 9	$Al_8O_3N_6$	85.7
21-R	7 : 8	$Al_7O_3N_5$	83.3
12-H	6 : 7	$Al_6O_3N_4$	80.0

*Bartrom only
^{t}Sakai only

M = Cation
X = Anion

Table 3. γ-ALON COMPOSITIONS

Oxynitide Spinel Formulas	Experimental Range Mole % AlN	References
$Al_{\frac{(64+x)}{3}} \boxed{S}_{\frac{(8-x)}{3}} O_{32-x} N_x$ $(0 \leq x \leq 8)$	40-27	McCauley (1978)
$Al_{\frac{(8+x)}{3}} \boxed{S}_{\frac{(1-x)}{3}} O_{4-x} N_x$ $(0 \leq x \leq 1)$	33-16	Lejus (1964)
$Al_{(2+\frac{x}{3})} \boxed{S}_{\frac{(3-4x)}{12}} O_{(3-x)} N_x$ $(0 \leq x \leq 3/4)$	50-33	Adams (1962)
$Al_7O_9N_1$	25	Kaufman (1979) Dormer (1981)
Al_3O_3N	50	Yamaguchi (1959) Henry (1969)
Al_3O_4	Misinterpreted	Yamaguchi (1950) Filonenko (1957) Vert (1957)

$\boxed{S}$ = Spinel cation vacancies
x = Limits from Al_3O_3N to Al_2O_3

Table 4. SPINEL STRUCTURES

	Stochiometric			Nonstochiometric		
Type	Normal	Inverse	Oxynitride*	γ-Oxynitride	γ-Oxynitride	γ-Alumina
Formula†	AB_2O_4	$B(AB)O_4$	BB_2O_3N	33.3 m/o AlN	35.7 m/o AlN	$B_{8/3}O_4$
Example	$MgAl_2O_4$	$MgFe_2O_4$	Al_3O_3N	Al_5O_6N	$Al_{23}O_{27}N_5$	Al_2O_3
Anion Sites 32 Total	(32) O^{-2}	(32) O^{-2}	(24) O^{-2} (8) N^{-3}	(27.44) O^{-2} (4.56) N^{-3}	(27) O^{-2} (5) N^{-3}	(32) O^{-2}
Cation Sites 16 (oct.)	(16) Al^{+3}	(8) Fe^{+3} (8) Mg^{+2}	(16) Al^{+3}	(14.88) Al^{+3} (1.12) [S]	(15) Al^{+3} (1) [S]	(13.3) Al^{+3} (2.7) [S]
8 (tet.)	(8) Mg^{+2}	(8) Fe^{+3}	(8) Al^{+3}	(8) Al^{+3}	(8) Al^{+3}	(8) Al^{+3}
Reference	Kingery (1976)		-	Goursat (1981)	McCauley (1978)	Lejus (1964)

*Not stable
†A = A^{+2}; B = B^{+3}; O = O^{-2}; N = N^{-3}

Table 5. ALUMINUM OXYNITIDE REACTIONS

	General Equations	T°C Required	References
1	$Al_2O_{3(s)} + AlN_{(s)} \longrightarrow \gamma\text{-}ALON_{(s)}$	≥1650°C	McCauley (1979) Hartmett (1981) Goursat (1976) Sakai (1978) Lejus (1964) Adams (1962)
2a	$Al_2O_{3(s)} + C_{(s)} + N_{(g)} \longrightarrow \gamma\text{-}ALON_{(s)} + CO_{(g)}$	≥1700°C	Rafaniello (1981) Ish-Shalom (1980)
2b	$Al_2O_{3(s)} + C_{(s)} + Air \longrightarrow \gamma\text{-}ALON_{(s)} + CO_{(g)}$	≥1700°C	Filonenko (1957) Vert (1957) Yamaguchi (1959)
2c	$Al_2O_{3(s)} + Al_{(\ell)} + N_{2(g)} \longrightarrow \gamma\text{-}ALON_{(s)}$	>1500°C	Michel (1966)
2d	$Al_2O_{3(s)} + Al_{(\ell)} + Air \longrightarrow \gamma\text{-}ALON_{(s)}$	>2045°C	Michel (1972) Collongues (1967)
2e	$Al_2O_{3(s)} + NH_{3(g)} + H_{2(g)} \longrightarrow \gamma\text{-}ALON_{(s)} + H_2O$?	≥1650°C	Collongues (1962)
3	$Al_{(\ell)} + Air \longrightarrow \gamma\text{-}ALON_{(s)}$	~1500°C	Michel (1972) Bouriannes (1974)
4	$AlCl_{3(g)} + CO_{2(g)} + NH_{3(g)} + N_{2(g)} \longrightarrow \gamma\text{-}ALON_{(s)} + CO_{(g)} + N_{2(g)} + HCL_{(g)}$	900°C	Silvestri (1975)

Table 6. ALUMINUM OXYNITRIDE SPINEL PROPERTIES

OPTICAL/DIELECTRIC		
IR Cut-Off	5.2 μm	Hartnett (1981)
Refractive Index	1.77→1.80	Corbin (1981)
Loss Tangent	0.004 (25°, 10^7 Hz)	Corbin (1981)
Dielectric Constant	8.5 (25°, 10^2 Hz)	Corbin (1981)
Magnetic Susceptibility	-0.34×10^{-6}/g (1300 Gauss.)	Yamaguchi (1959)
MECHANICAL		
Hardness	1650→1800 Kg/mm^2	Rafaniello (1981)
Elastic Modulus	47×10^6 psi	Corbin (1981)
Poisson Ratio	0.249→0.263	Corbin (1981)
Fracture Strength	35→50 x 10^3 psi	Corbin (1981)
THERMAL		
Thermal Shock (ΔT_c)	175 ± 5°C	Corbin (1981)
Thermal Conductivity (RT)	0.026 cal (cm·S·K°)$^{-1}$	Sakai (1978)
Thermal Expansion Coeff.	7.59×10^6/°C (25°-1000°)	Sakai (1980)
	5.23×10^6/°C (20°-2000°)	Corbin (1981)
Thermal Diffusivity	0.043 cm^2/S (300°K)	Sakai (1978)
	0.027 cm^2/S (400°K)	Sakai (1978)
Specific Heat	0.169 cal/g·°K (300°K)	Sakai (1978)
	0.252 cal/g·°K (450°K)	Sakai (1978)
CHEMICAL		
Melting Point in N_2	2165 ± 15°C	McCauley (1981)
Oxidation Resistance	Protective Layer ~1200°C	Corbin (1981)
	Starts at ~650°C	Goursat (1976)
Chemical Attack	Stable Versus Acids & Bases	Yamaguci (1959)

III. Research Objective

The objective for this research is to better understand the formation of Aluminum Oxy-nitride Spinel (γ-ALON). This will be done by conducting a thermodynamic analysis of various γ-ALON reactions and comparing to experimental results. The reactions which will be experimentally evaluated include: oxy-nitridation of liquid aluminum, plasma sprayed Al_2O_3 in nitrogen, and powder mixtures of Al_2O_3 + AlN, Al_2O_3 + Al, and Al_2O_3 + C.

Powder mixtures of Al_2O_3 + AlN are commonly used for producing γ-ALON, therefore this reaction will be investigated in greater detail. For this reaction a thermodynamic evaluation of the equilibrium vapor pressures for Al_2O_3 and AlN as a function of temperature and atmosphere will be conducted.

This thermodynamic information will be used to analyze experimental results from Al_2O_3 + AlN powder mixtures and diffusion couples. The data collected will include weight changes, microstructures, surface chemistry, and percent of γ-ALON formed.

IV. Experimental Procedure

IV.1. Powder Preparation

The powders used in this work are listed in Table 7, along with their as-received impurity levels. The aluminum, carbon, and αAl_2O_3 powders were used as-received while the AlN and γ-Al_2O_3 powders were ball milled before using.

IV.1.1 Aluminum Nitride

Figure 8 shows the particle size distribution of this powder as determined by the Micromerities X-ray Sedigraph.® This powder was chosen because of its relatively high purity (99.8%). In order to improve its physical characteristics, ball milling was performed which resulted in obtaining sizes similar to the γ-Al_2O_3 powder, also shown in Fig. 8. The milling operation consisted of using 100g of powder in a 500 ml Nalgene ® jar, with thirty five 5/8" diameter 99.9% αAl_2O_3 milling media, and 110 cc absolute ethanol. Samples were removed from the jar at various time intervals to monitor the reduction process (Fig. 8). After 64 hrs. of milling, the size distribution was much narrower and the median particle size was 1.25 μm. During this milling operation, the wear of the Al_2O_3 media added oxygen to the powder as Al_2O_3. This oxygen content had to be factored into the powder mixtures in order to obtain the desired compositions. The oxygen content as determined by neutron activation analysis, increased from 2.1 weight % O in as-received material to 7.7 weight % after 64 hrs. of milling. Once milled the powder was dried at 200°C for 1 1/2 hrs. to remove any remaining alcohol, 400°C for

24 hrs. to remove hydrated species, then heated at 600°C for 3 hrs. to remove carbon picked up from the plastic milling jar. The 600°C firing was required because after heating at 400°C, the plastic picked up from the jar decomposed leaving a black carbon residue on the powder. An 800°C temperature was tested, but it resulted in a weight gain which signified simultaneous carbon removal and oxidation. A TGA (Thermo Gravimetric Analysis) of similar powder milled 67 hrs (Fig. 9) revealed oxidation can start as low as 800°C, but is minimal after 3 hours at this temperature, therefore, at 600°C I am confident only the carbon is removed. This TGA data shows how easily AlN powder can be oxidized at temperatures above 800°C so care must be used when conditioning it. The theoretical percent weight change which results upon complete oxidation of AlN ($^{+}$24.4%) agrees well with the TGA results if the Al_2O_3 in the starting AlN is factored in. X-ray diffraction results, confirm the equation in Fig. 9 because αAl_2O_3 is the only product of oxidation. The final step is to put the powder into a blender for several seconds to break up the large granules which formed during drying. The XRD pattern of this powder after preparation reveals AlN and a trace (~5%) of αAl_2O_3. Powders ball-milled for 64 hours were used in the diffusion couple experiments while a similar batch milled for 67 hours was used in the powder mixture studies. Even though the 67 hour batch was milled longer, the particle sizes were not reduced as much as the 64 hour batch and the oxygen pick up (5.38 w/o) was less. This result is attributed

to the 67 hour milling having slightly more alcohol present, thereby reducing the efficiency of the grinding operation. Figure 10c,d shows SEM photos of both these powders after milling.

IV.1.2 Gamma Alumina

This powder was ball-milled 24 hours under the same conditions as the AℓN powder. Ball-milling was used to produce fresh surfaces for reaction, and reduced the particle size as shown in Fig. 8. The X-ray diffraction trace of this powder show it to be a poorly crystalline material with the peaks being very broad and of low intensity. SEM photographs of two lots of the prepared powder are shown in Fig. 10a,b. Notice how many large (>1μm) rectangular particles still remain after milling. From these SEM photographs γ-Al_2O_3 appears coarser than AℓN while the opposite is true from the Sedigraph data. It appears the AℓN size from the Sedigraph was largely influenced by agglomerates.

IV.1.3 α-Al_2O_3, Carbon, Aluminum

The other powders used in this study are shown in Fig. 11. All these powders were used as-received thus no further conditioning was performed.

The αAl_2O_3(GE) powder (Figs. 11a,b) consist of aggregates approximately 1-μm in size which contain particles on the order of 0.2 μm. From the photographs it appears that the particles are bonded together by some neck growth. Both the carbon and aluminum (Fig. 11c,d) powders are much coarser

powders. The carbon has particles over 20 μm in size but also contains many fine <1 μm particles. The Aluminum powder, which is very smooth shaped, consists of ~20 μm particles having a very narrow size distribution.

IV.2 Sample Preparations

In this study two kinds of samples were prepared: pellets of powder mixtures to form γ-ALON and pellets of the individual components to use in diffusion couples. Each will be discussed separately.

IV.2.1 Powder Mixtures

Three powder mixtures to form γ-ALON were made; they consisted of γAl_2O_3 + AℓN, αAl_2O_3 + C, and αAl_2O_3 + Aℓ. In Appendix I the calculations used for determining the proper amount of the components to mix are described.

The γ-Al_2O_3 and AℓN (milled 67 hrs.) powders were mixed in 150g batches using mechanical and magnetic stirring as shown in Fig. 12. First the powders were dry mixed in a bowl and then slowly added to alcohol in the plastic beaker. Additional powder and alcohol was added until a viscous solution formed. This solution was mixed for three hours, then dried by turning on the heater and raising the water temperature to about 60°C causing the alcohol to evaporate. Water was used to protect the plastic jar from melting. While evaporation was occurring both the spin bar and stirrer were kept running so segregation would not occur during drying. When the mix became thick and the spinbar could no longer turn,

the sample was removed from the plastic jar, dried in an oven at 100°C for 5-hrs, put into a blender for 2 seconds to break up agglomerates, and further heated at 600°C for 3 hours to remove any plastic pickup. Since much smaller amounts of the αAl_2O_3 + C and αAl_2O_3 + Al mixtures were made (~2 grams), they were dry mixed with a magnetic stirrer for approximately one hour. The γ-Al_2O_3 + AlN mixture was isostatically pressed at 25,000 psi in 1.5 cm diameter rubber bags, while the other mixtures were pressed at 2000 lbs in a 5/16" diameter uniaxial die. Figure 13 shows SEM fracture surfaces of the γ-Al_2O_3 + AlN powder mixture after pressing. The rectangular shaped γ-Al_2O_3 particles can be readily seen.

IV.2.2 Pure Components

Diffusion couple samples required a flat surface so a uniaxil press was used. Three powders were pressed in this manner αAl_2O_3, γ-Al_2O_3, and AlN (milled 64 hours). The AlN was pressed in a 5/16 dia. die at 3000 lbs while the Al_2O_3 powders were pressed in a 3/4" dia. die at 9000 lbs. The smaller AlN samples were originally prepared to aid in observing surface features which may form due to Al_2O_3-AlN interactions at high temperatures; all subsequent experiments also used this sample size.

IV.3 Sample Firings

Using a variety of furnaces, samples were heated at various temperatures and in different atmospheres depending on the desired data. Low temperature studies (<1400°C) were

carried out in air or flowing nitrogen atmospheres. Reactions in nitrogen were done in a horizontal alumina muffle tube furnace. Oxygen in the N_2 was removed by passing it through a copper gauze oxygen getter at 600°C. The gas was kept flowing during the heating, temperature hold, and cooling of all samples. Reactions in air were fired either in a refractory brick box furnace or the Al_2O_3 muffle tube furnace depending on sample size restrictions and temperatures.

The high temperature studies (>1400°C) were carried out either in a graphite induction heated furnace or a refractory metal resistance heated furnace, both of which were operated in nitrogen or argon atmospheres. In all cases, the experiments were done at ~1 atmosphere pressure in flowing gas (~$\frac{1}{2}$ ℓpm) purified by passing through oxygen getters.* In an attempt to improve the stabilization of temperatures, samples were inserted in boron nitride crucibles. This helped in the induction furnace which, because of manual controlling, often drifted in temperature. Figure 14 shows the design of the induction furnace. It consists of a 2.7" tube of calcium stabilized cubic zirconia which has several vertical and horizontal cuts. These cuts allow expansion and contraction of this outer shell due to the thermal expansion of the zirconia. The next layer is zirconia felt** roughly .1" thick which is used as an insulating layer, it was replaced regularly because the furnace was operating near this materials

*Diamond Tool and Die Co.
**Zircar Products Inc.

stability limit. The inner layer is a tube of graphite with a 0.2" wall thickness which acts as the susceptor for the induction heating. This furnace assembly is inserted in a quartz tube fitted with gas tight end fixtures then placed between the induction coils. Temperatures as high as 2300°C were easily obtained with this furnace design. Samples were centered by using a rod of Boron Nitride (BN) hollowed out to decrease thermal conductivity effects. They were inserted in a BN crucible atop the rod. As shown in Fig. 14, it was built so three samples could be simultaneously heated above each other. The top sample temperature was monitored with an optical pyrometer by sighting through a prism and holes in the furnace and BN covers. The temperature was corrected for reflection by glass surfaces and for temperature gradients which occur within the crucible as determined by calibration studies. Control of this furnace was generally $\pm$15°C with a heating rate such that it would take just short of one hour to reach temperature. The initial cooling rate was obtained by shutting the power to the induction coils.

The temperature in the refractory metal (tungsten mesh heating elements) furnace was controlled within $\pm$1°C by using a microprocessor controller and a Tungsten-Rhenium thermocouple. In order to have the only difference between the two furnaces be the presence of carbon from the susceptor, they were run using the same, heating and cooling rates, BN crucible, gases and gas flow rate.

IV.4 X-Ray Photoelectron Spectroscopy (XPS or ESCA)

IV.4.1 Advantages

The advantages of using XPS in this study are threefold. One, since γ-ALON is composed of low atomic number elements, techniques such as microprobe analysis and EDAX are not useful since they do not detect for oxygen or nitrogen. In this work I want to be able to monitor, semi-quantitatively, the presence of these two elements in order to understand the reaction process. Two, since this technique is surface sensitive (5-50Å depth) it could give insight to how the surface composition of the particles in a mixed compact change. This change would be due to surface diffusion or evaporation/condensation of one phase onto the other. Three, XPS is capable of determining binding energy differences between oxygen in one material and another, hence phase identification is possible. Once a data base of the binding energies for each element in my phases of interest (AℓN, αAl_2O_3, γ-ALON) are obtained, then analysis of heated powder mixtures should enable determination of the surface phases. This may help determine how AℓN and αAl_2O_3 are transported.

IV.4.2 Theory

The principles of XPS have been reviewed in terms of its application to glass and ceramics (59). This technique involves the excitation of a sample with a known monochromatic x-ray radiation ($h\nu$) then monitoring the kinetic energy (KE) of the emitted core level electrons. The binding energy (BE)

for the electron is found by subtraction

$$BE = h\nu - KE \ .$$

These binding energies are specific for each element, and therefore allow chemical analysis of the material. Since core electrons are analyzed, all elements except hydrogen can be detected. When precise high resolution analysis are conducted, slight variations in the binding energy reveal information on the chemical state of the element. If reference data is available, phase analysis can be conducted on the sample by these variations.

Since electrons have very short mean free paths, they are easily scattered. This requires XPS analysis to be conducted in high vacuum (at least 8×10^{-8} Torr). The x-rays used for excitation penetrate into the bulk of the sample and excite electrons there; however these become scattered and lose their specific energies. Only electrons which originate at the surface (depth of 5Å-50Å) are able to exit from the material and keep their specific energies, thus the technique is utilized for surface analysis.

There are several limitations with this type of analysis, some are due solely to using nonconducting materials. An intrinsic limitation is the spatial resolution of analysis ($>1mm^2$), this is because x-rays cannot be focused. The information obtained therefore gives the average composition over a very large region. Also, this method is only able to detect elements present in a concentration greater than

.1 atomic %.

Since the materials of interest are nonconductors, the emission of electrons produces a (+) charge on the surface which cannot be removed. For XPS this charging generally becomes stable, and results in a uniform shift in the binding energy values. The best way to analyze XPS data which has surface charges is to record the differences between, in our case, the oxygen auger peak and the binding energy peaks (60). This method eliminates charge effects and allows comparisons between samples. The auger peak occurs due to a decay process which involves filling the core hole formed by x-ray excitation with an outer electron and emission of another electron. Other problems such as sample heating and phase dissociation may become important factors in the analysis.

IV.4.3 Sample Preparations

Samples for analysis with XPS were prepared slightly different depending on the desired information. A sintered γ-ALON sample was cut and polished with this new surface analyzed. This sample is to supply base information on the bonding energies for aluminium, oxygen, and nitrogen in γ-ALON. Other samples for base information includes the starting powders of AℓN and αAl_2O_3 along with an unheaded powder mixture. The powder samples were prepared by pressing in a uniaxial press, cleaned with 600 mesh SiC polishing paper; then analyzed. The analysis of fired AℓN + γAl_2O_3 powder mixtures were obtained on fracture surfaces in order to evaluate the

surface composition of the particles as a function of temperature, for my analysis only samples which showed interparticle fracture could be used. Samples which show trans granular fracture would give data on the inside of the particles and not the surfaces. All samples analyzed using XPS were also observed with an SEM to check the type of fracture.

IV.5 High Temperature Plasma

An attempt was made to produce aluminum oxy-nitrides from alumina powder heated in a nitrogen plasma. A coarse grained (~20 μm) α-Al_2O_3 powder (Bay State PP-33) was used to avoid clogging the feeding mechanism. The major impurities of this starting material are listed in Table 7. Argon gas was mixed with the α-Al_2O_3 powder to help feed it into the plasma.

Two different methods were used to collect the powder as it was sprayed from the plasma; spraying onto a glass microscope slide held approximately 3 inches from the nozzle and spraying into a glass beaker with its bottom approximately 12 inches from the nozzle. Both techniques supplied enough powder for analysis by x-ray diffraction and optical microscopy.

IV.6 Data Collected

The data collected on samples includes: % weight changes, bulk density, x-ray diffraction analysis, and microstructural analysis using SEM (scanning electron microscopy),

reflected and transmitted microscopy.

For mixed powder samples it was required to determine precisely the percentage of γ-ALON which formed. This was done by measuring the intensity of selected AℓN, αAl_2O_3, and γ-ALON peaks, obtaining the ratios between them, then matching these values to a calibrated standard. The specifics of this procedure along with information on making the reaction standards are listed in Appendix 2.

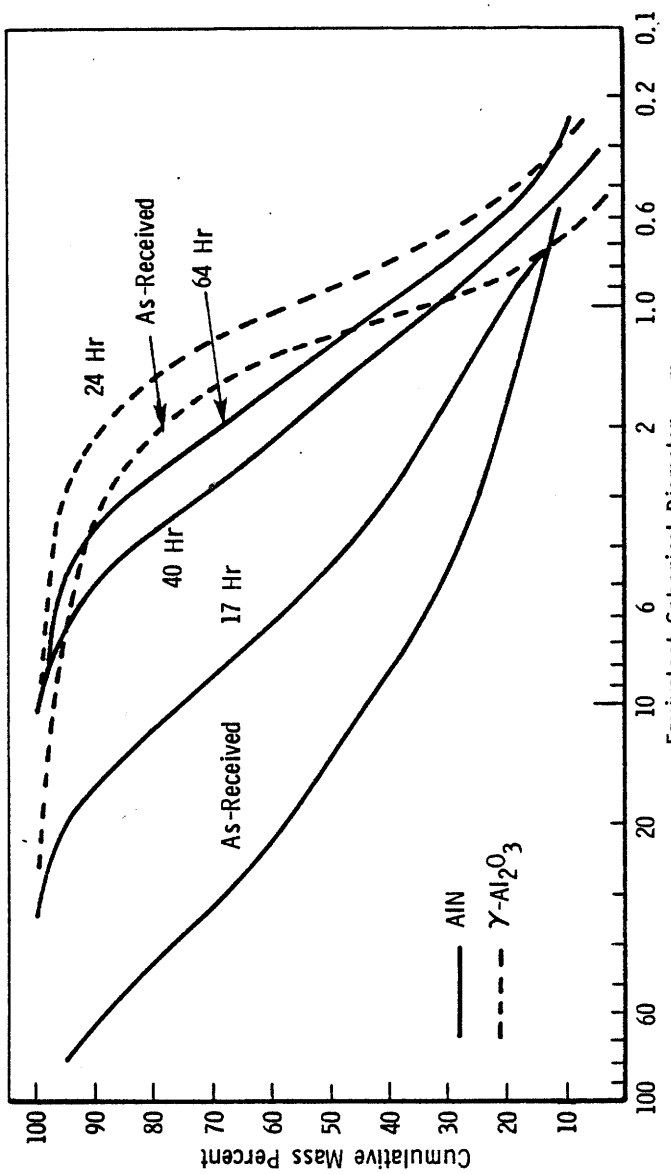

Figure 8. AlN AND Al_2O_3 MILLING

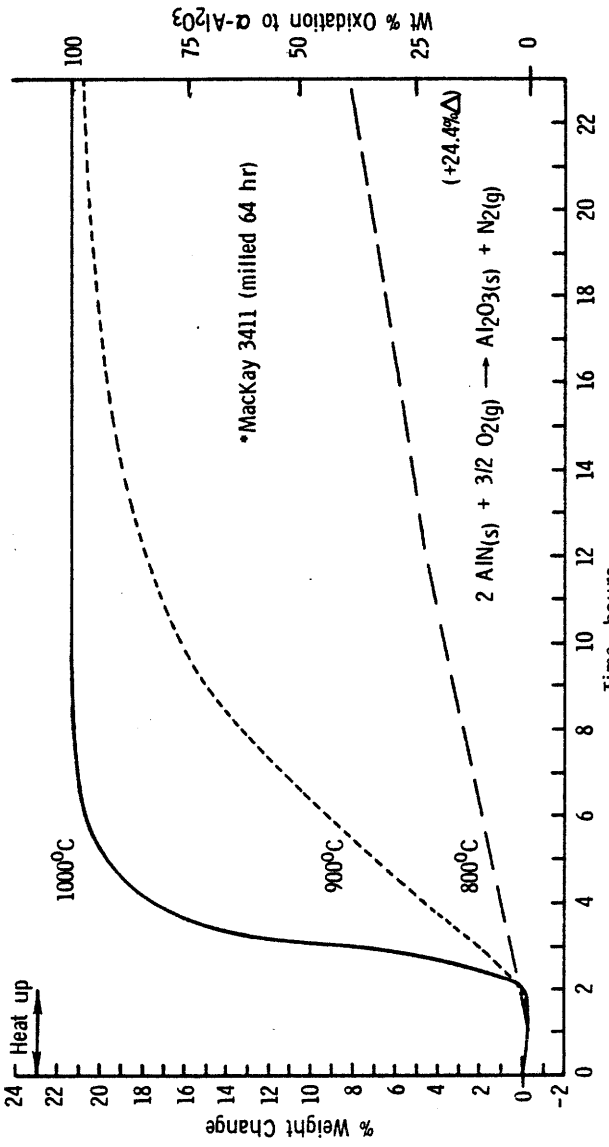

Figure 9. TGA OF AlN* POWDER IN AIR

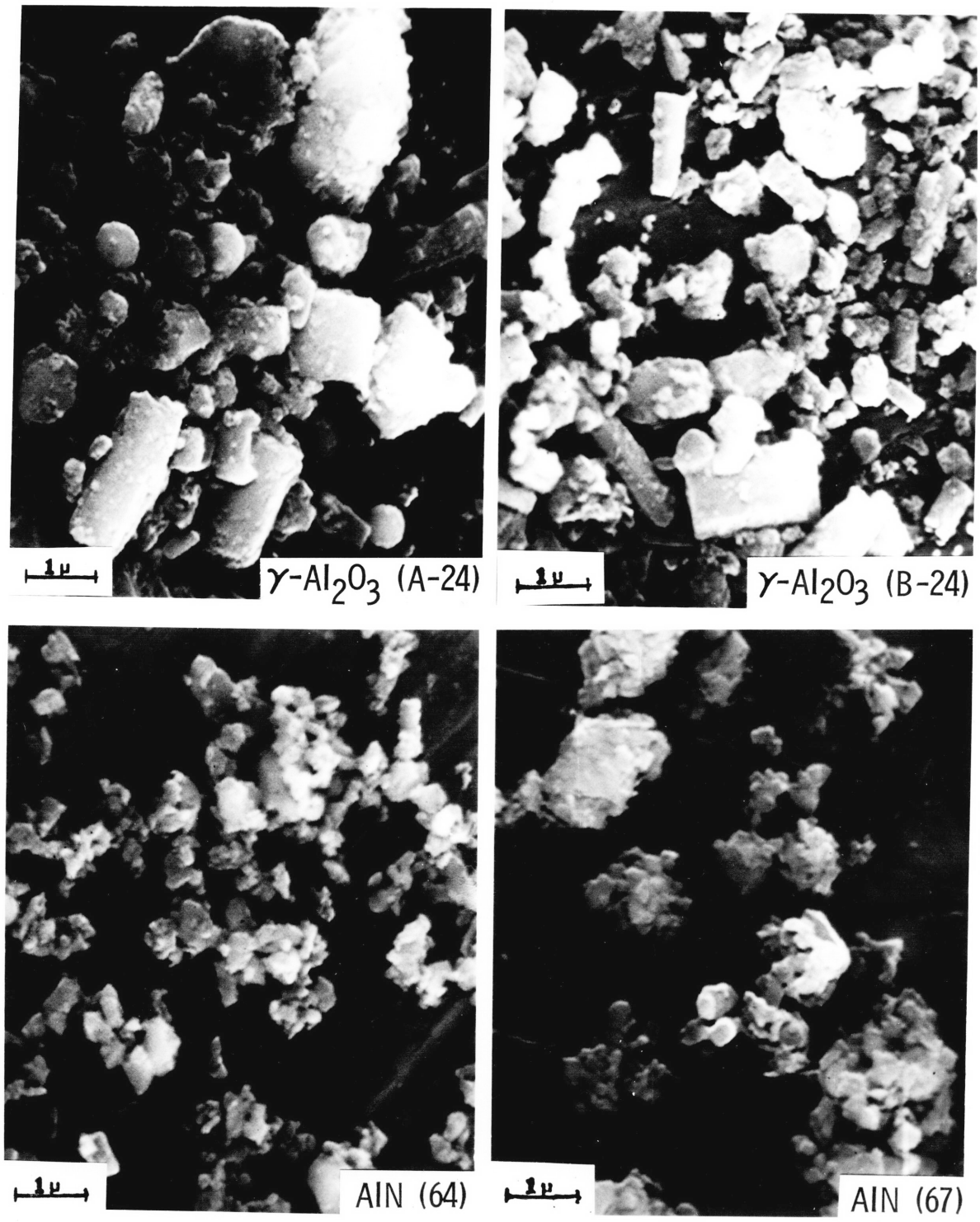

Figure 10. SEM OF STARTING POWDERS

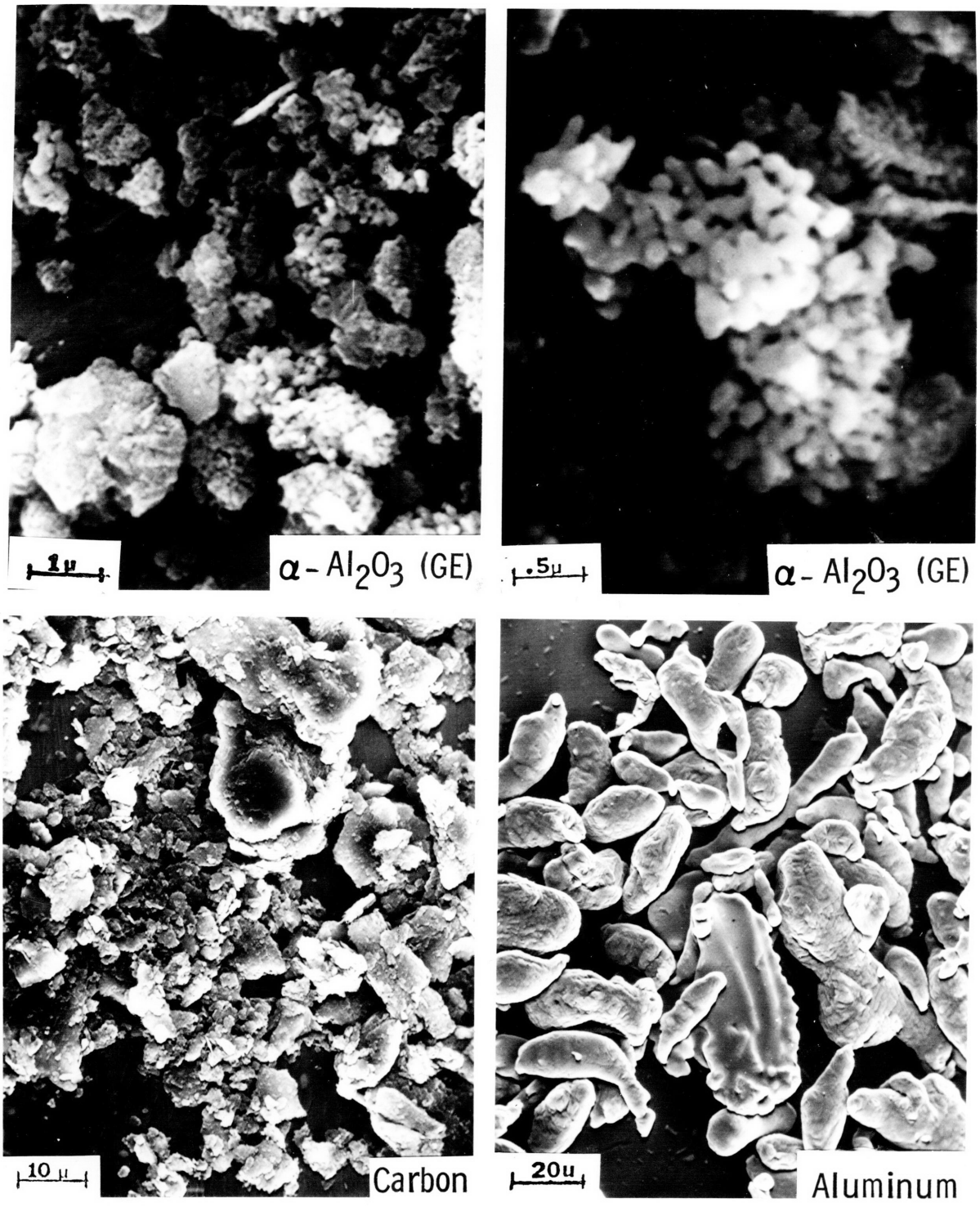

Figure 11. SEM OF STARTING POWDERS

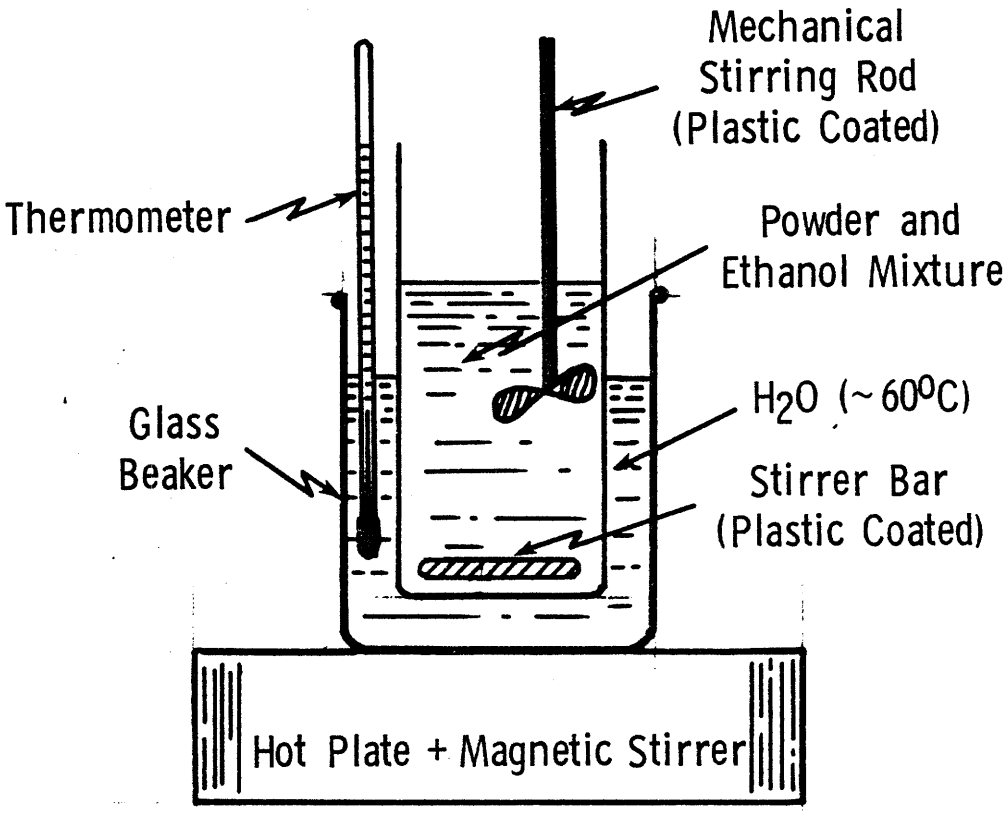

Figure 12. MIXING ARRANGEMENT

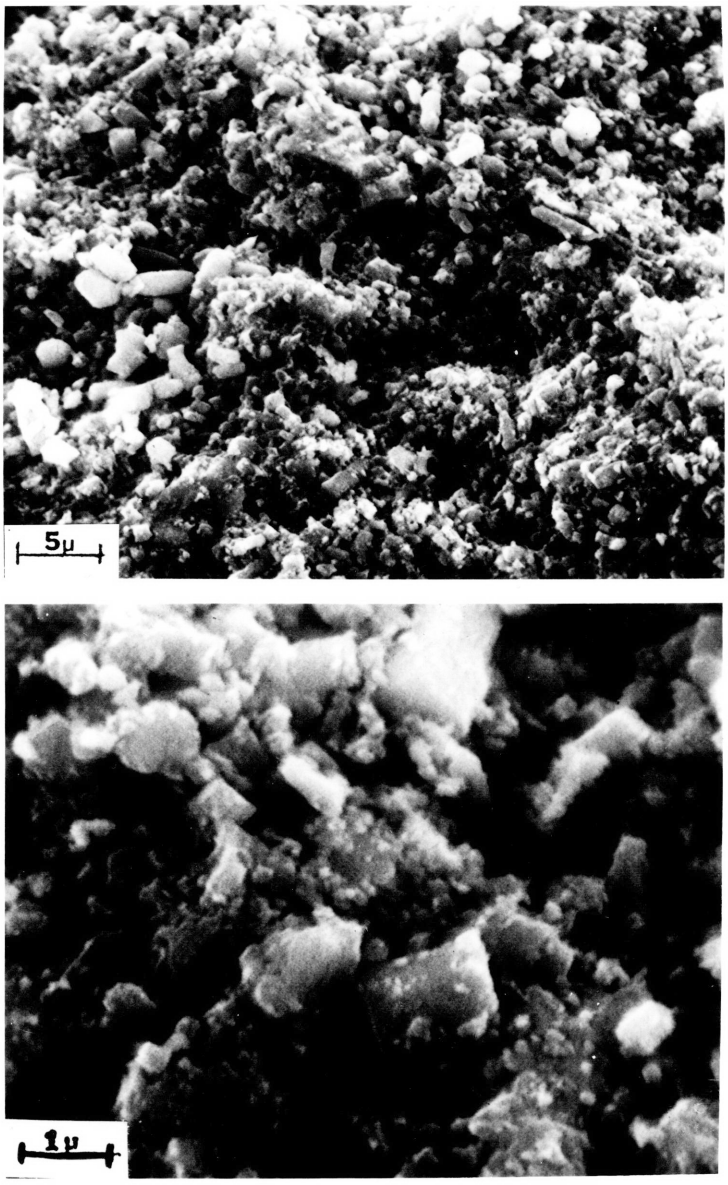

Figure 13. SEM OF γ-AL_2O_3 + AIN AS-MIXED POWDER PELLET

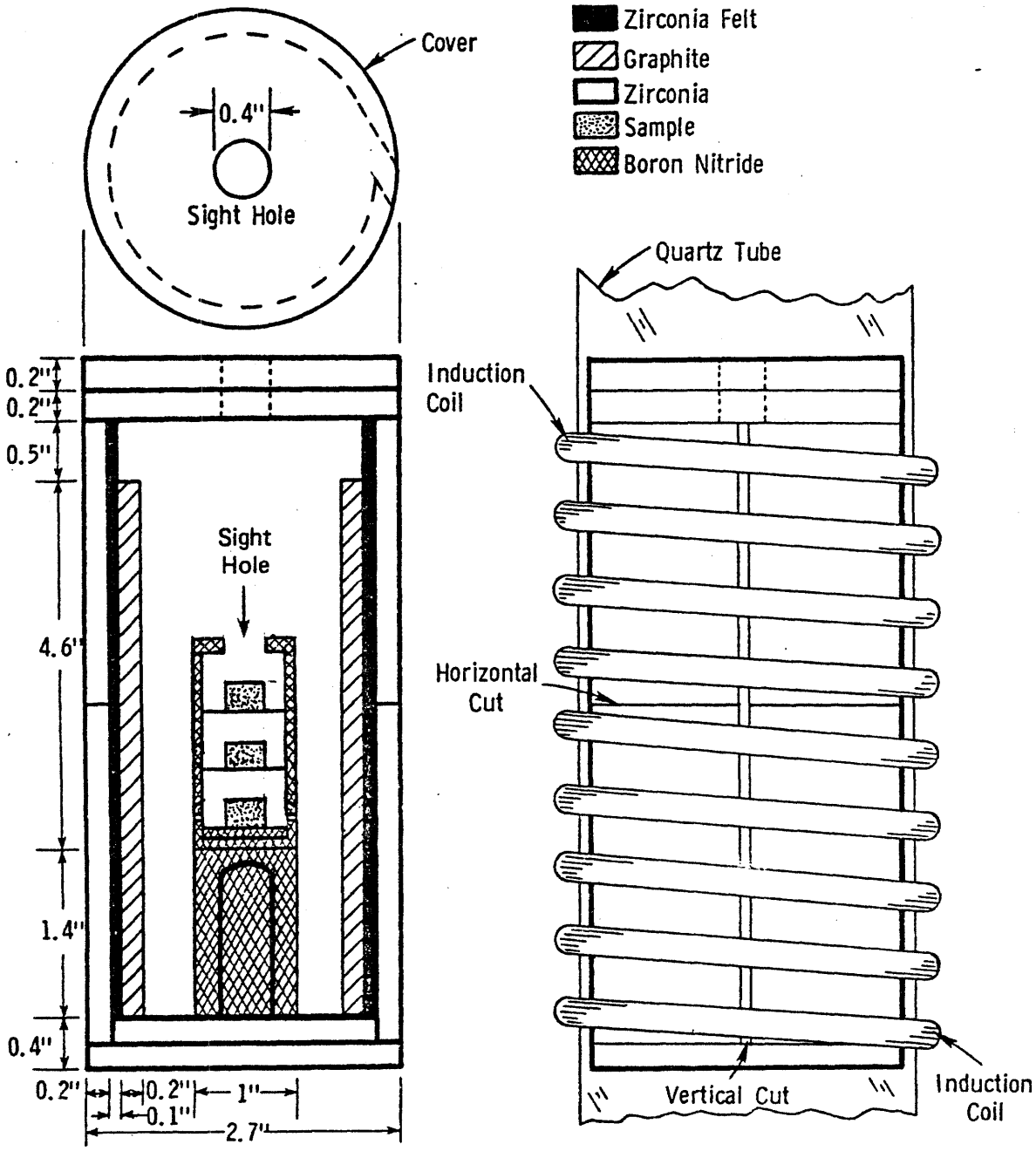

Figure 14. INDUCTION FURNACE DESIGN

Table 7. CHEMICAL ANALYSIS OF STARTING POWDERS

	AlN* MacKay (3411)	γ-Al_2O_3* Cerac (1566)	α-Al_2O_3† GE (30AS3)	α-Al_2O_3† Bay St. (PP-33)	Al† Fisher (A-559)
Ca	<0.01	<0.01	0.008	0.052	0.01
Cr	~0.05	~0.01	0.008	0.008	0.008
Cu	~0.05	~0.05	<0.01	<0.01	<0.01
Fe	~0.1	0.1-0.5	<0.006	0.16	0.23
Mg	0.01-0.05	~0.05	0	0	0
Si	0.05-0.1	0.1-0.5	0.013	0.15	0.06
Ti	~0.001	<0.01	0	0.017	0
Zr	0	<0.01	0	0.02	0

*Semiquantitative emission spectroscopy
†ICP-quantitative emission spectroscopy

V. Results

V.1 Powder Mixtures

As discussed in the procedure section several powder mixtures were utilized to produce γ-ALON. These included γAl_2O_3 + AℓN, αAl_2O_3 + Carbon, and αAl_2O_3 + Aluminum mixtures. The γAl_2O_3 + AℓN mixtures were heated in nitrogen and argon atmospheres in both the graphite induction and tungsten resistance furnaces to test the effect of atmospheres on weight loss and microstructure. Table 8 summarizes the data from these experiments. The other powder mixtures were heated only in the tungsten resistance furnace in nitrogen; these results will be discussed separately.

V.1.1 Al_2O_3 + AℓN Mixture

(a) Graphite Furnace. This furnace was used with a nitrogen atmosphere to investigate how time and temperature can effect weight changes, γ-ALON formation, bulk density, and microstructural development. One run was also performed in Argon for comparative purposes.

(i) Time Effects. The samples were heated for times ranging from 0.5 hr to 2.0 hrs at 1605°C and 1745°C. After heating at 1605°C for 0.5 hrs, there is negligible further weight loss by extending the heating time. It is known that γAl_2O_3 tends to adsorb moisture from the laboratory environment; therefore some of the weight loss may be attributed to this. At 1745°C the amount of weight loss tends to decrease with longer heating times. It appears some kind of reaction,

possibly with N_2, is occurring which may account for this. After heating for 0.5 hrs at 1745°C, 80% of the sample has converted to γ-ALON, increasing to 88% after one hour.

The fracture surface microstructure of samples fired for various times at 1605°C are shown in Fig. 15. When compared with Fig. 13 of the prefired mixture there is a dramatic change in microstructure, although no spinel has formed. The sample now consists of almost spherical shaped particles partially bonded together, with a much narrower size distribution than the original mixture. The sintering which occurred is seen as particle coarsening due to the elimination of the fine fraction in the original sample. The average grain size has slightly increased to nearly 1 μm, prior to firing the particles were predominantly smaller than this size. Heating for two hours at this temperature has minimal microstructural effect other than a slight increase in particle size.

(ii) Temperature Effects. Temperatures in the range of 1530°C to 1775°C were investigated and compared after heating for one hour. The reaction temperature to form γ-ALON from both 30m/o and 35.7m/o powder mixtures lies between 1605°C and 1745°C. The reaction to form αAl_2O_3 from γ-Al_2O_3 powder generally occurs at much lower temperatures (~1000°C). The % weight loss appears to have a maximum near 1605°C for both 30m/o and 35.7m/o compositions. This may signify some reaction of the powder with the atmosphere at higher temperatures.

Figure 16 shows the rather dramatic change in micro-

structure for a 35.7m/o composition as a function of temperature. Even at 1530°C (Fig. 16a) there is a large change in microstructure from the original as pressed sample (Fig. 13). At 1605°C (Fig. 16b) some fine particles (~.25 μm) still remain with larger ~1.0 μm diameter particles. Bonding between the particles has occurred but a significant amount of open porosity still remains. Faceted particles are produced at this temperature (Fig. 16b). At 1775°C (Fig. 16c) the sample is 80% reacted to γ-ALON with a large increase in sintering. This sintering is exhibited by the different mode of fracture in this sample (transgranular vs intragranular) and an apparent decrease in porosity. This sample also exhibits neck growth between the particles, typical of intermediate stage sintering. Figures 17a,b show identical microstructural development for 30m/o samples.

(iii) Atmosphere Effects. One 30m/o sample was heated at 1685°C in argon for one hour. When compared to samples heated under similar conditions in nitrogen, this sample has a much higher weight loss, with the same amount of γ-ALON formed. On comparison of Fig. 17b with 17c, the microstructural differences due to atmospheres are seen. In argon, the sample has a much coarser microstructure even though it was fired at a lower temperature. The agglomerates are roughly twice the size of those found when heated in N_2. Much more neck growth has occurred, although the structure is still at the intermediate stage. The bulk density data (61) (on small samples) shows a slightly higher (~7%) density when fired in

argon than in nitrogen.

From the above data on firing γ-Al_2O_3 and AlN in the graphite furnace, the results can be summarized as follows:

(1) Temperatures greatly influence the amount of γ-ALON which form, higher temperatures do not necessarily mean larger weight losses, and the microstructure coarsen as the temperature increases.

(2) Argon produces larger weight losses, a coarser microstructure, and slightly higher densities than nitrogen.

(3) The time effects the percent of γ-ALON which forms, has a small effect on the microstructure but longer times can mean weight loss increases or decreases depending on the temperature.

(b) Tungsten Metal Furnace. Samples of 30m/o were heated in this furnace at 1650°C or 1800°C in nitrogen or argon atmospheres. When heated in nitrogen the same weight loss occurs at 1650°C and 1800°C. However, 97% of the sample reacted at 1800°C while only 15% reacted at 1650°C. Figures 18a,c show the fractographs of these samples—similar microstructural relationships to those discussed for the graphite furnace results are also seen here. In this case at 1650°C the temperature is high enough to cause some γ-ALON formation and neck growth. Also, at 1650°C both transgranular and intragranular fracture occur. This temperature is near a transition between reaction/no reaction and intergranular/transgranular fracturing. Minimal particle growth but much neck growth has occurred between 1650°C and 1800°C.

When fired in argon, a much larger weight occurs at 1800° than at 1650°C. The percent of γ-ALON to form at 1800°C is nearly 95%, while at 1650°C only a trace forms. One of the AℓN "polytype-like" phases also appears at 1850°C but may only be occurring due to the kinetics of the oxide-nitride reaction. The relationship between microstructure and temperature (Fig. 18b,d) are similar to that when firing in nitrogen, but the argon fired samples have a coarser microstructure.

From the above results we can summarize:

(1) Samples fired in argon exhibit larger weight losses and larger grain sizes than those fired in nitrogen.

(2) At 1650°C nitrogen appears to promote the reaction since over 3 times more γ-ALON is formed than in argon for the same time period.

(3) At 1800°C the percent of γ-ALON formed is similar in both atmospheres.

(4) The bulk density for the sample heated at 1800°C in argon is slightly (~6%) higher than that heated in nitrogen.

(c) General Effects. Due to uncertainties in calibrating the induction furnace temperature, it is difficult to compare the results of the two furnaces. However, some general observations can be made:

(1) The weight losses in nitrogen in the tungsten furnace are higher than in the carbon furnace.

(2) The weight loss in an argon atmosphere are also

slightly higher in the tungsten furnace.

(3) Argon tends to produce samples with higher densities and with coarser microstructures than nitrogen in both furnaces.

V.1.2 Al_2O_3 + Carbon Mixture

Samples of this powder mixture were heated in flowing nitrogen at 1360°C for 75 hours in an alumina muffle tube furnace or 1650°C for one hour in the tungsten furnace. After the lower temperature heat treatment XRD revealed only αAl_2O_3 present; it seems a leak may have developed allowing air into the furnace. This allowed oxidation of the carbon leaving only Al_2O_3. If no air was present and no reaction occurred both Al_2O_3 and carbon should have remained.

The diffraction pattern of this mixture after heating at 1650°C shows αAl_2O_3 AℓN, and γ-ALON. The simultaneous reduction/nitridation of alumina should lead only to γ-ALON as determined by the phase diagram. It seems as if AℓN is an intermediate product for producing γ-ALON by this reaction. Since the three phases still remain the reaction has not gone to completion. The large weight loss results from oxidizing the carbon to carbon monoxide gas.

V.1.3 Al_2O_3 + Aluminum

This powder mixture was also heated at 1360°C for 75 hrs in an alumina muffle furnace or 1650°C for 1 hour in the tungsten metal furnace. Air leakage into the furnace at

1360°C also appears to have occurred. When this sample was analyzed by XRD only α-Al_2O_3 remained. This would only occur by oxidizing the Al metal powder to Al_2O_3.

After heating at 1650°C for one hour in nitrogen, the resulting phases were αAl_2O_3, AlN, and γ-ALON. Again, AlN has formed as an intermediate product. Since αAl_2O_3 and AlN remained, the reaction has not gone to completion. The weight gain for this reaction is expected since the aluminum liquid (T_m ~ 660°C) is nitrided at these temperatures.

The amount of γ-ALON to form under the same conditions of firing for these two powder mixtures (Al_2O_3 + Al, Al_2O_3 + C) are different. The Al_2O_3 + C mixture produces more γ-ALON than Al_2O_3 + Al, but more AlN is found in the Al_2O_3 + Al. In both cases the reducing agent (C or Al) is not found in the sample after firing.

V.2 Diffusion Couples

V.2.1 Individual Components

A series of diffusion couple type experiments were conducted to help understand the material transport which occurs during the Al_2O_3 + AlN reaction. The data obtained from these samples includes: surface and bulk phases of the pellets, surface microstructures, and weight losses. These data were taken from samples prepared under various temperature, atmosphere, and furnace conditions. Initial data was obtained on the individual components (αAl_2O_3, γAl_2O_3, AlN) to compare with the results when the Al_2O_3 and AlN

pellets are in contact. In all diffusion couple studies the samples were held at the desired temperature for two hours. Data from these experiments are listed in Table 9.

(a) Al_2O_3. Pressed disc of both γ-Al_2O_3 and α-Al_2O_3 were investigated. At 1715°C in the carbon furnace with a nitrogen atmosphere, the surface of the γ-Al_2O_3 started to form γ-ALON after the γ-Al_2O_3 to α-Al_2O_3 conversion. As shown by Rafaniello (38) carbon in contact with Al_2O_3 in a nitrogen atmosphere can produce γ-ALON. To determine my source of carbon, either residue from milling in plastic or from the furnace wall, an unmilled α-Al_2O_3 powder was fired under identical conditions. This sample had an even larger amount of γ-ALON formed at the surface. The α-Al_2O_3 may appear more reactive than γ-Al_2O_3 due to the finer particle size. This sample was then ground and reanalyzed by XRD which showed only α-Al_2O_3 present. This shows that the oxynitride is only a surface feature which would result if the carbon came from the susceptor. When another α-Al_2O_3 pellet was fired under the same conditions except in an argon atmosphere, no γ-ALON formed. This shows that nitrogen readily reacts with α-Al_2O_3 in the presence of carbon at this temperature. The α-Al_2O_3 was also fired in the refractory metal furnace in nitrogen at 1650°C; no γ-ALON formed even though for A&N-Al_2O_3 powder mixtures, γ-ALON can form under these conditions. It appears the combination of carbon from the graphite furnace and nitrogen is required to produce the γ-ALON on the α-Al_2O_3 samples.

Weight loss data can also be very useful in observing the effects of both the atmosphere and the furnaces on the samples. Under similar conditions γ-Al_2O_3 has a much lower weight loss than α-Al_2O_3. This can be attributed to the volitiles picked up by these samples in the laboratory environment. As already mentioned, α-Al_2O_3 has a much higher surface area, therefore more volatiles will adsorb on the powder. The largest weight loss for α-Al_2O_3 is in the combination of carbon furnace and nitrogen, (-4·56), followed by carbon furnace and argon (-2.31) and then refractory metal furnace and nitrogen (-1.78).

(b) AlN. Data on AlN was only obtained with an argon atmosphere in the refractory metal furnace. This should give the maximum weight loss because a nitrogen atmosphere will suppress the AlN decomposition reaction. As shown by XRD no reaction occurred between the Al_2O_3 picked up from ball milling and the AlN. This is rather surprising since under similar conditions a small amount of γ-ALON formed in the reaction of AlN and Al_2O_3 powder mixtures.

V.2.2 Al_2O_3 & AlN Couple.

The data collected on these samples includes weight changes and X-ray diffraction analysis of the pellet surfaces facing each other. The data are summarized in Table 9.

(a) Graphite Furnace. Since Al_2O_3 can react with graphite and N_2 gas to form γ-ALON, as shown with α-Al_2O_3 pellets, only preliminary information was obtained using this furnace.

A run at 1800°C in N_2 produced much densification of the γ-Al_2O_3 sample along with a color change from white to light grey. X-ray diffraction of the bulk phases revealed the γ-Al_2O_3 pellet converted to α-Al_2O_3 while γ-ALON plus AlN was in the AlN pellet. Since the AlN did contain some Al_2O_3 from the milling operation, some of the γ-ALON formed is attributed to this source.

When a similar run was performed in Argon, the surfaces (analyzed by XRD) show γ-ALON formed on both samples. The amount of γ-ALON in the AlN cannot be explained solely from the Al_2O_3 picked up upon milling. It appears a mutual transport of oxygen and nitrogen is occurring. As with the results in a nitrogen atmosphere, no bonding occurred between the pellets.

When the γ-Al_2O_3 and AlN samples were heated in this furnace in a nitrogen atmosphere at 2000°C, several interesting results were formed; most importantly is the fact no bonding occurred between the samples. This tends to disagree with the presence of a eutectic between γ-ALON and αAl_2O_3; no markings from a liquid or large vaporization has occurred. The surface phases include over 90% γ-ALON on the α-Al_2O_3 pellet and a mixture of γ-ALON plus AlN on the AlN pellet. The α-Al_2O_3 pellet was nearly transparent on the outer rim but not in the center. Figure 19 is a cross section through this pellet, a crack (indicated by arrows) has influenced the transparency in this region. Figure 20 is a reflected light micrograph showing both the porosity and grain size

distribution of this sample near the crack. The crack has influenced both the grain size and porosity near it. This could be a result if it acts as a vacancy sink or the atmosphere in the crack might have been influential in keeping the grain size small. The grain size changes dramatically from about 75 μm, at the outer portion of the sample to over 300 μm, then back to about 100 μm at the center. All the porosity is trapped at the center of the sample.

Polarized transmitted light shows that all grains in the reflected light micrographs are not cubic and XRD of the crushed sample shows only α-Al_2O_3. Since no cubic phase was found in the sample, the γ-ALON found by XRD of the surface must have consisted of a very thin (micron range) outer layer which was destroyed in the grinding and polishing operation for microscopic observation.

(b) Tungsten Furnace. Several experiments were done in a refractory metal furnace to eliminate the problem of a strong reducing carbon atmosphere which tends to form γ-ALON as discussed. These runs were done at 1650°C, this turned out to be a low for much significant γ-ALON formation. In the AℓN & γ-Al_2O_3 powder mixtures, between 5 and 15% γ-ALON formed but in the reaction couples only a trace of γ-ALON formed on the Al_2O_3 pellet in N_2. It is interesting to note again that no γ-ALON has formed in the AℓN which contains ~5w/o Al_2O_3 from the milling operation.

Even though the 1650°C diffusion couple data yielded minimal γ-ALON reaction information, the weight changes of

the samples are of interest. Since the refractory metal furnace was controlled to $\pm$ 1°C and all the runs at 1650°C were identical (including heating rate, time at temperature, and cooling rate) the % weight change values are very informative. For the AlN pellets the sample fired in nitrogen instead of argon has a significantly smaller (0.7 vs 1.57) percent weight loss. The two AlN samples (not in contact with Al_2O_3) have identical values (1.69, 1.72) while the sample in contact with Al_2O_3 in argon has a slightly lower value (1.57). When the Al_2O_3 disc is heated separately in nitrogen (1.78) or argon (1.77) or in contact with AlN in argon (1.77) the weight changes are identical at 1650°C. However, when heated in contact with AlN in nitrogen there is a significantly larger weight loss (2.22). It appears that the combination of AlN and nitrogen causes a reaction that affects the weight loss of this sample. This latter sample is also the only one to form any γ-ALON at 1650°C.

A run was conducted at 1650°C by suspending the AlN pellet over the α-Al_2O_3 pellet with tungsten wire. The distance between the samples was roughly 2-3 mm. No reaction or transport of material appears to have occurred—this is no different than when they are in contact at 1650°C.

In order to obtain more information about the transport of material, two experiments were conducted at 1800°C for three hours in argon. Since argon will allow more vaporization of AlN, it was used to maximize AlN transport and give information as to how this can affect the reaction.

One of the experiments was done with the two pellets touching while the other was done by suspending the AlN as previously described.

The results from the pellets in contact are significantly different from the same set up when heated at 1650°C for 2 hrs. The weight losses at 1800°C were much larger for Al_2O_3 (-1.77 vs -3.58)and the AlN (-1.57 vs -9.82) pellets. X-ray diffraction analysis of the touching surfaces show 100% γ-ALON on the AlN pellet and γ-ALON, α-Al_2O_3, 12-H, plus another undetermined phase on the α-Al_2O_3 pellet. The texture of the α-Al_2O_3 surface was different where the AlN pellet was resting on it. Photomicrographs of the as-fired surface using reflected light microscopy are shown in Fig. 25. The α-Al_2O_3 surface away from the AlN is shown in Fig. 25a as having a grain size near 75 μm. Figure 25b is of a transition region between the edge and the position where AlN and Al_2O_3 are in contact. It appears as if some kind of dendritic growth is starting to cover the large grains which can still be seen. Where the AlN was in contact with the Al_2O_3, the sample is very porous with deep open cavities signifying much vaporization. Figure 25c is this region but due to the shallow depth of field of the microscope used, a sharp image was not obtained. It appears AlN catalized the vaporization of Al_2O_3 below it and also causes rapid grain growth of either α-Al_2O_3 or γ-ALON (not determined) away from it.

The experiment done with AlN and α-Al_2O_3 spaced apart

used a different AℓN powder in order to eliminate the α-Al_2O_3 in AℓN due to milling. The same as-received AℓN powder was used, but instead of milling to reduce the particle size, it was classified to separate the particles less than ~5 μm which were then used. The results show no γ-ALON formed on either pellet. The α-Al_2O_3 pellet had a glassy appearance on the side toward AℓN but X-rays only show α-Al_2O_3, Fig. 25 d shows this surface. When compared with the previous sample it has a uniform surface with a grain size near 20 μm. This is dramatically different from the sample heated at 1650°C under identical conditions which has had no substantial grain growth. The larger grain size may be due to activation by the AℓN vapors, but this is only speculative since XRD shows only α-Al_2O_3. The weight loss for this sample is significantly less (-4.06 vs. -3.58) than when its touching AℓN. The weight loss for AℓN is high partly due to the long time exposure to the laboratory environment for this fine powder. Also at this elevated temperature AℓN decomposes much more readily, especially in argon.

V.2.3 Summary

From the previous data it appears the furnace and atmosphere are very influential in both forming γ-ALON and weight changes. This is mainly due to different oxidation potentials in the graphite and tungsten furnace, nitrogen reacting with Al_2O_3 and suppressing the AℓN decomposition

reaction, and argon allowing AℓN vaporization.

V.3 Aluminum Reaction

As previously discussed, both Michel (27) and Bouriannes (45) were able to produce aluminum oxynitrides by heating aluminum metal in air at high (≥1500°C) temperatures. It is also known that during the processing of aluminum ingots a dross forms on the exposed molten aluminum (T_m~ 660°C) surface—this dross contains both Al_2O_3 and AℓN (62) It seems nitrogen in the atmosphere become reactive at high temperature and result in nitridation or even oxynitridation rather than just oxidation of aluminum.

Several experiments were carried out which exposed molten aluminum to air for extended times in order to try and duplicate the previous results. Attempts were tried with the aluminum powder previously described (Fig. 11d). The results at 800°C and 1000°C for up to 90 hrs only show α-Al_2O_3 forming. One very interesting feature with this material is the powder never appears as if melting had occured, even though the sample was >300°C above its melting point. The oxide layer which develops over the surface keeps the molten aluminum from flowing by acting as an impermeable shell on each particle. In order to try and solve this problem a solid ingot (~10 grams) sample was heated at 1000°C for 90 hours. Similar results occurred as with the powder; no obvious liquid occurred and a thick flaky oxide layer formed. This layer was removed by brush-

ing and analyzed by XRD to be pure αAl_2O_3.

It appears at these temperatures γ-ALON cannot form from molten aluminum even though this reaction has a large free energy of formation. The previous results described must be largely due to using higher temperatures, or as discussed by Bouriannes, effected by the pressure of the atmosphere—or there was a more reducing atmosphere present which was able to remove the thin oxide layer from the aluminum.

V.4 X-ray Photoelectron Spectroscopy (XPS or ESCA)

As mentioned in the preceding section, base data was obtained from αAl_2O_3 powder, sintered γ-ALON, AℓN powder, and an as-mixed 35.7m/o AℓN powder pellet. The other sample analyzed was a 35.7 m/o AℓN sample fired at 1530°C for 1 hr.

Figure 21 shows the survey scans for γ-ALON and α-Al_2O_3. This figure shows the number of electrons detected over a range of binding energies. Both samples show the presence of aluminum, oxygen and carbon. The carbon is due to atmospheric contaminants which adsorb on the powder surface. The γ-ALON sample also contains nitrogen (as expected), argon (from sputtering), and magnesium (probably due to contaminants from a sample fired at the same time). The magnesium and nitrogen contents appear equal from the plot but the magnesium content is actually one tenth that of nitrogen. This result is due to the different atomic sensitivity factors (ASF) for the two elements.

Figure 22 shows the survey scans for the 35.7 m/o AℓN powder mixture and 35.7 m/o fired at 1530°C. Both of these samples contain aluminum, oxygen, carbon, and nitrogen. The reason for the very weak signal off the fired sample is because a fracture surface is being observed. The roughness of this surface (Fig. 51a) tends to block the path of some emitted electrons, therefore less reach the detector. The AℓN powder (milled 64 hrs) is not shown since the only elements detected were aluminum and oxygen. This is due to the milling process which forms a thick oxide layer on the particles. The reason the 35.7m/o as-mixed sample does show nitrogen is that it contains AℓN milled 67 hrs which has a substantially lower oxygen content (5.4% vs 7.7%) and, therefore, a thinner oxide layer.

To obtain estimates on the ratios between various elements at the surface, the heights of the elemental peaks and the ASF factors are used. Using the data from α-Al_2O_3 as an example, the method will be described. From the survey scan the ratio of the height of the oxygen (1s) peak to the aluminum (2P) peak is 6.8/1. Using the formula of Al_2O_3 and the respective ASF values (O = .63, Aℓ = .11), an expected ratio can be developed:

$$\begin{array}{l} 3 \times .63 = 1.89 \quad \text{oxygen} \\ 2 \times .11 = \ .22 \quad \text{aluminum} \end{array} \qquad \frac{O}{A\ell} = \frac{8.6}{1}$$

For Al_2O_3 the experimental and expected ratios are similar. This same procedure was used to determine the values in Table 10. The large differences between theoretical and

obtained values for γ-ALON and 35.7 as-mixed can be explained. The surface analyzed for γ-ALON was previously relief polished with alumina for microscopic evaluation. This polishing must have contaminated the sample with alumina or caused oxidation due to heat generation during grinding. Either method is capable of contaminating the 5-50 Å surface region analyzed. As previously discussed the low nitrogen content in the 35.7 mixture is due to the oxide layer on the AℓN powder.

High resolution scans were used to accurately determine the binding energy of oxygen (1S), oxygen (auger), and aluminum (2P) electrons. It was hoped this information could aid in determining the phases present on the particle surfaces along with the information of the chemical species. Because charging is a problem on nonconducting samples, it is best not to use the actual binding energies but what is called the auger parameter (60). Table 11 lists the binding energies obtained and the corresponding auger parameters. Since there is negligible difference between the auger parameters of oxygen or aluminum in α-Al_2O_3 and in γ-ALON, it will not be possible to determine the phases present at the particle surfaces.

V.5 High Temperature Plasma

The αAl_2O_3 powder used in this work is listed along with its major impurities in Table 7. X-ray diffraction analysis of this starting material revealed it as a combina-

tion of α-Al_2O_3 and another phase. To determine this phase a computer assisted search through the powder diffraction file found Nitrosyl Aluminum Oxide ($NO_2O \cdot 11\ Al_2O_3$) (63). Studies by Radzilowski and Kummer (64) have determined this phase to have a β-alumina type structure.

After passing this powder through the plasma X-ray diffraction revealed the same two phases remained. The nitrogen plasma had no affect on the phase composition of the powder. Powder collected on the slide and in the beaker were both analyzed with polarized transmitted light microscopy; this confirmed that no cubic phases were formed. The sample collected on the glass slide was obviously molten upon contact, with the particle sizes between 1-5 μm. The sample collected in the beaker was significantly coarser (~20 μm) and did not appear to have melted. It seems the slide only collected small particles which were molten and rejected the large solid particles, while the opposite was true for the beaker which collected the large particles and not the fine fraction. It was noticed when collecting in the beaker fines were being blown out over the rim due to the force of the plasma spray.

The powder collected in the beaker was further annealed at 1650°C for one hour in nitrogen. If the sample was indeed $NO_2O \cdot 11Al_2O_3$ it may have been possible to form an oxynitride spinel by a higher temperature anneal. The results showed complete conversion to α-Al_2O_3. There is strong doubt that the phase $NO_2O \cdot 11Al_2O_3$ was actually present

in this powder even though its diffraction pattern explained most of the non αAl_2O_3 peaks. This is because the nitrogen did not remain after annealing in the nitrogen atmosphere.

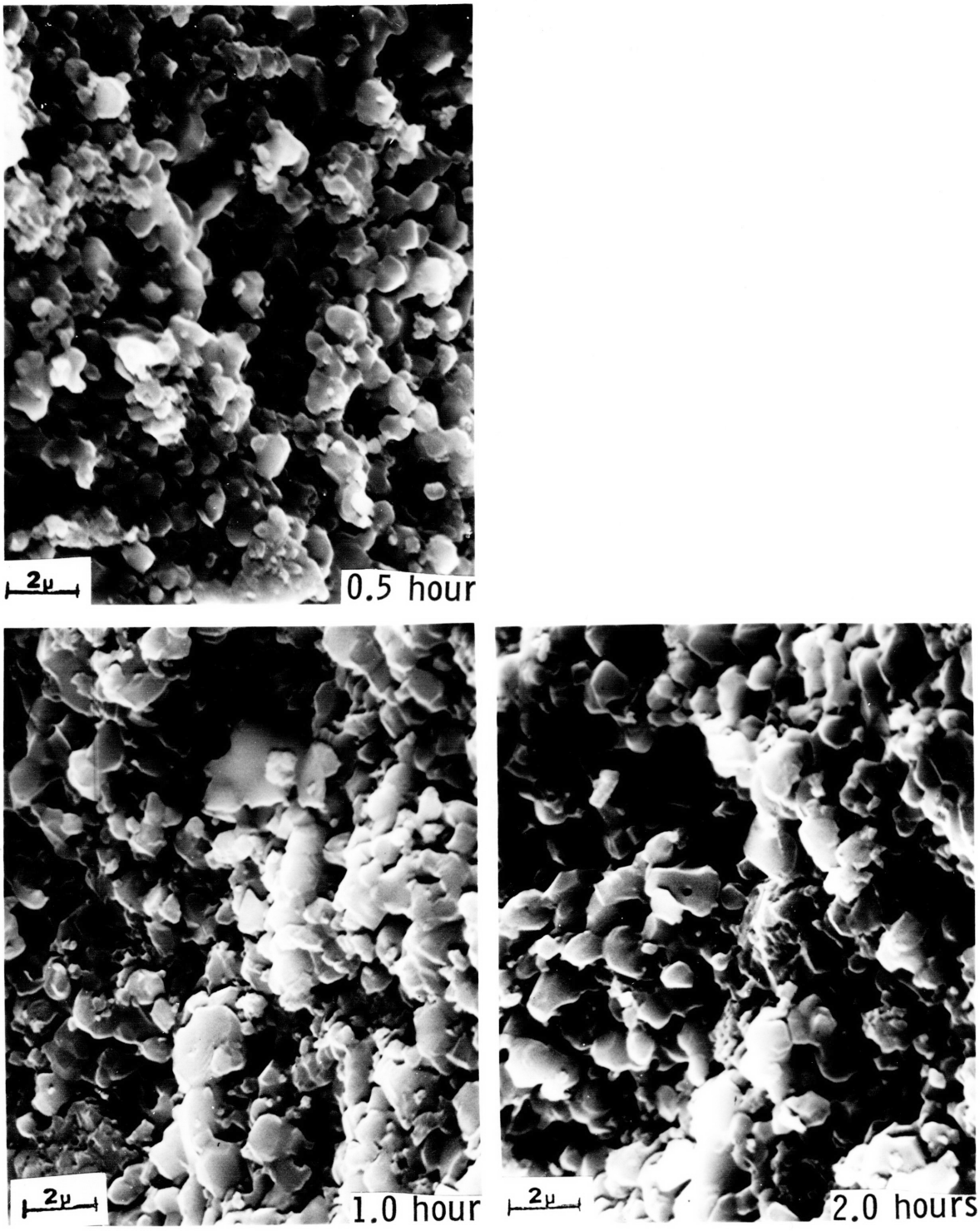

Figure 15. FRACTURE SURFACE SEM OF 30 m/o AlN, CARBON FURNACE, NITROGEN, 1605°C

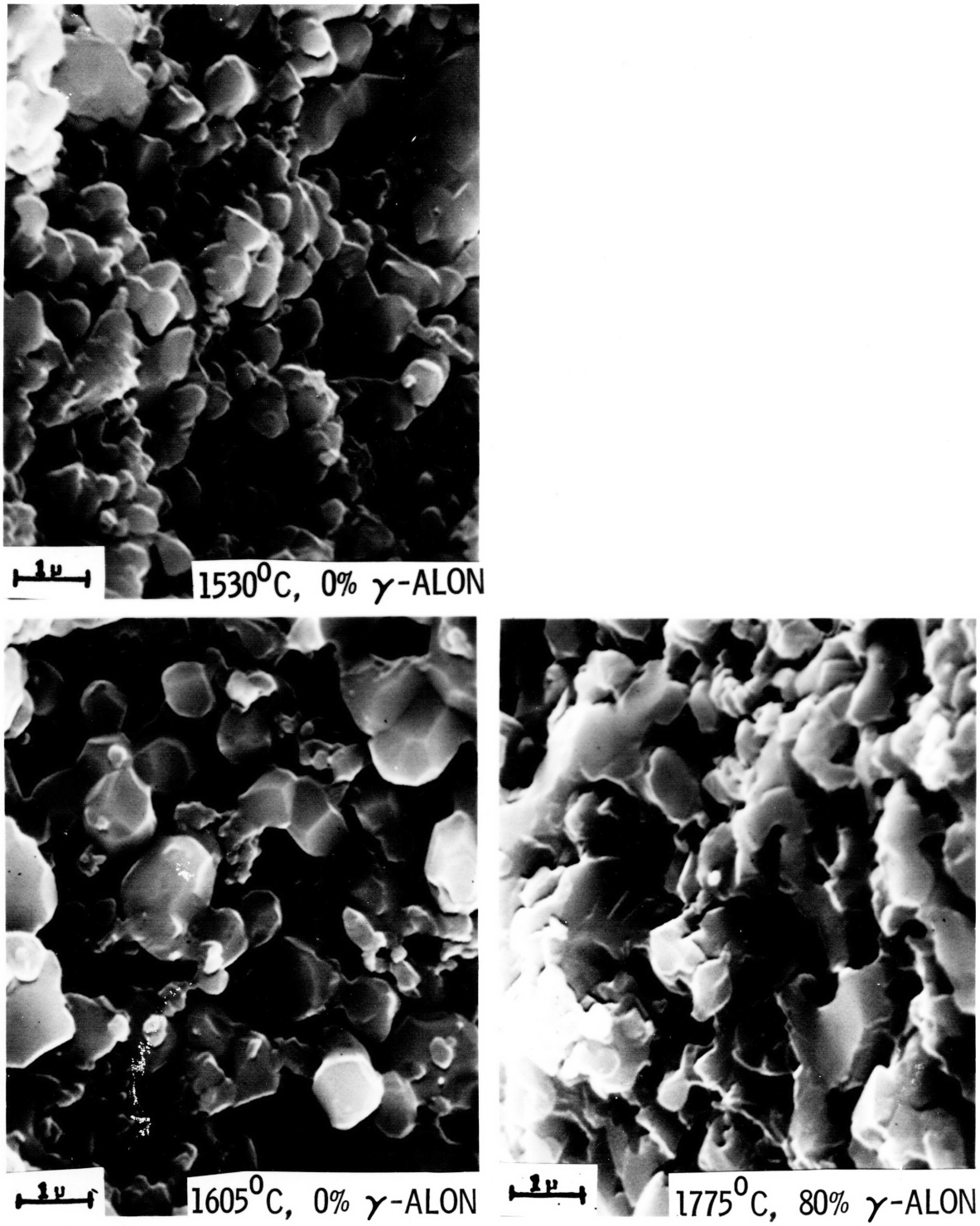

Figure 16. FRACTURE SURFACE SEM OF 35.7 m/o AIN, CARBON FURNACE, NITROGEN, 1 HOUR

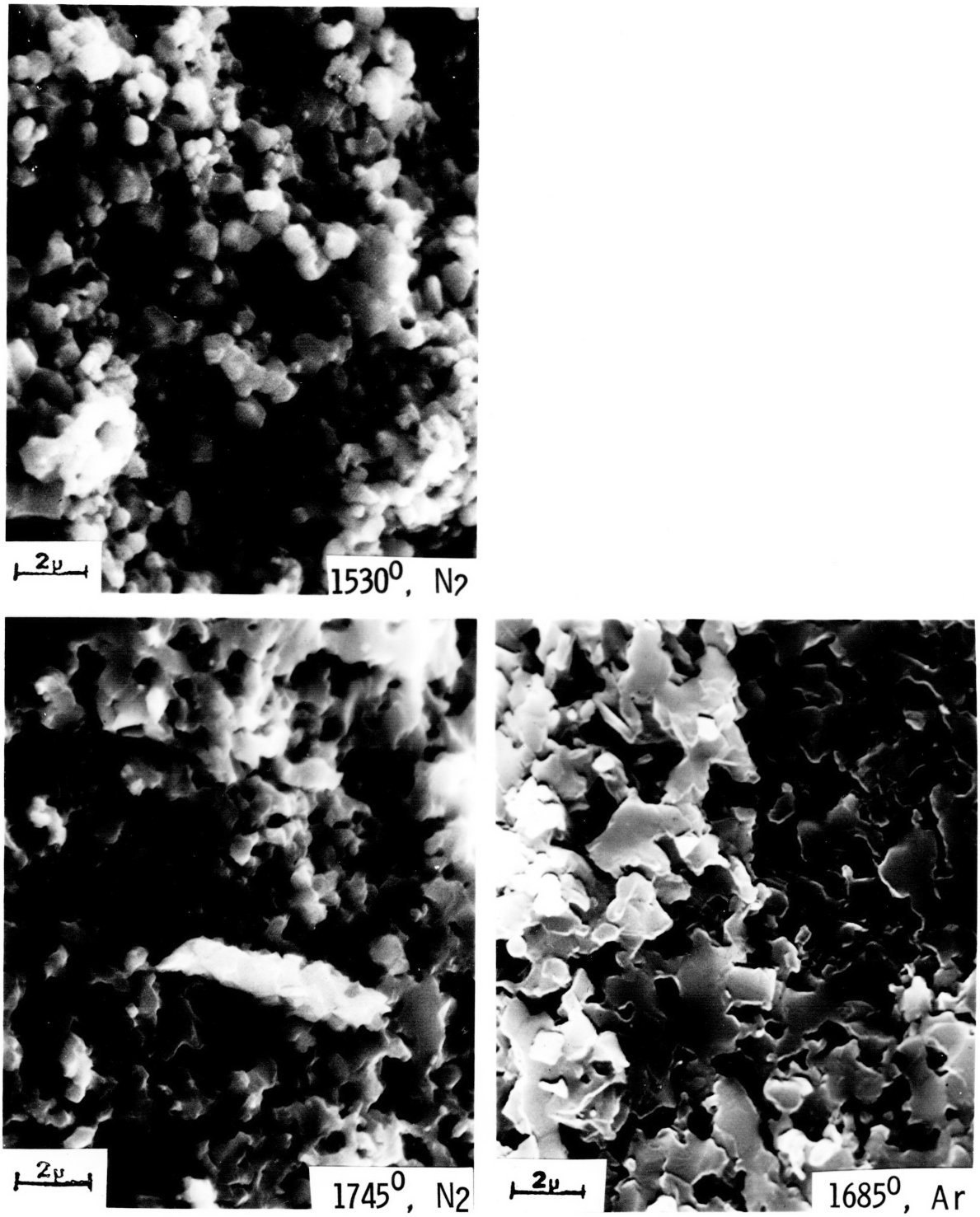

Figure 17. FRACTURE SURFACE SEM OF 30 m/o AlN, CARBON FURNACE, 1 HOUR

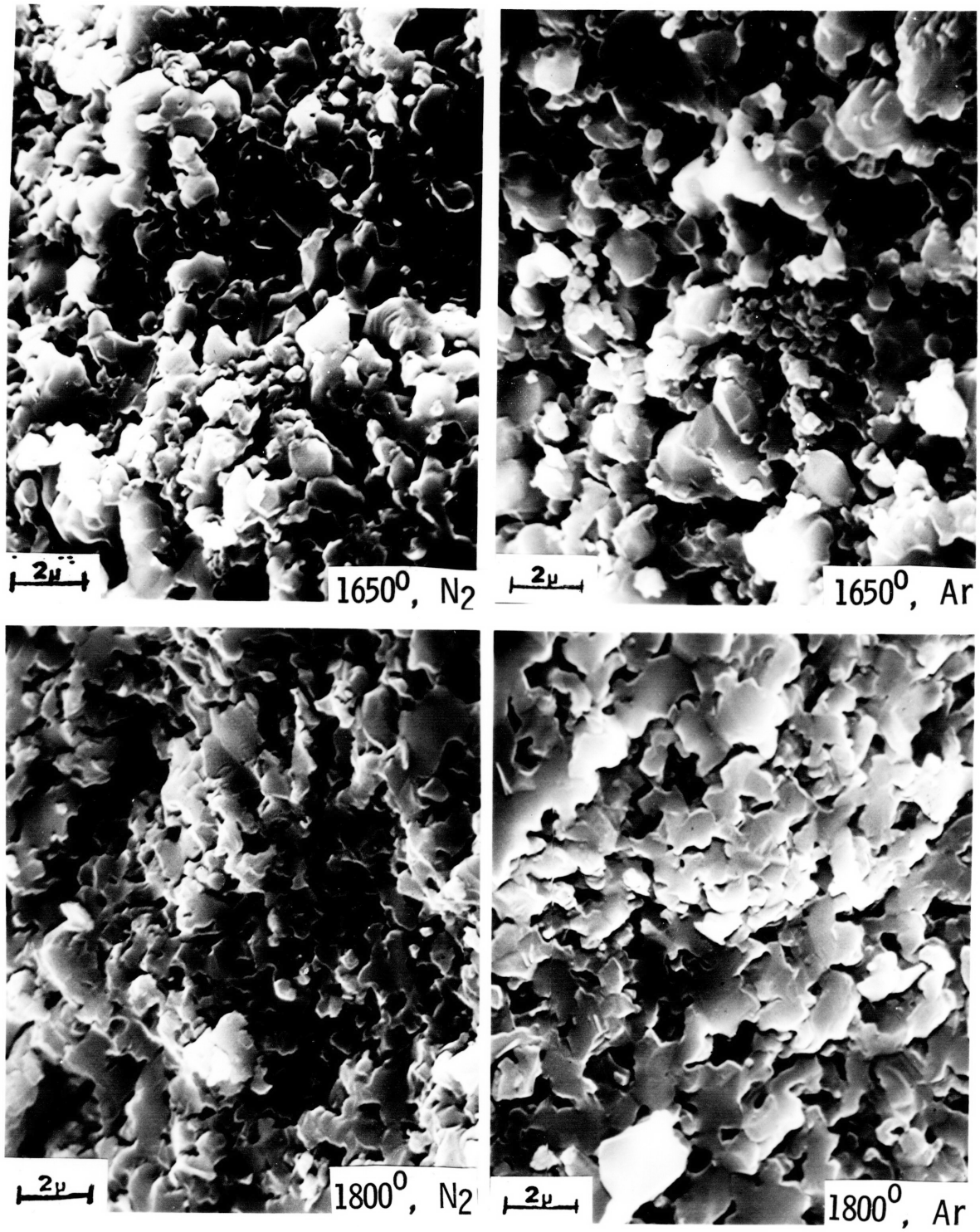

Figure 18. FRACTURE SURFACE SEM OF 30 m/o AlN, REFRACTORY METAL, 1 HOUR

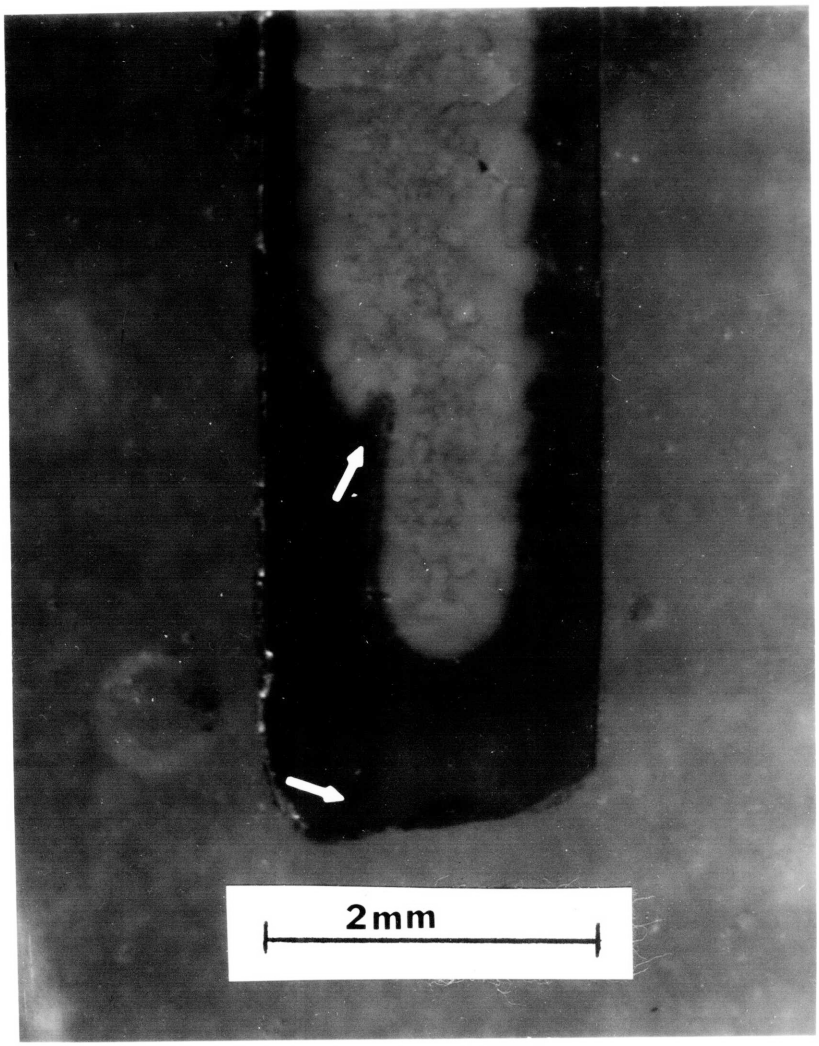

Figure 19. α-Al_2O_3 PELLET, GRAPHITE FURNACE, N_2, 1905^oC, IN CONTACT WITH AIN PELLET

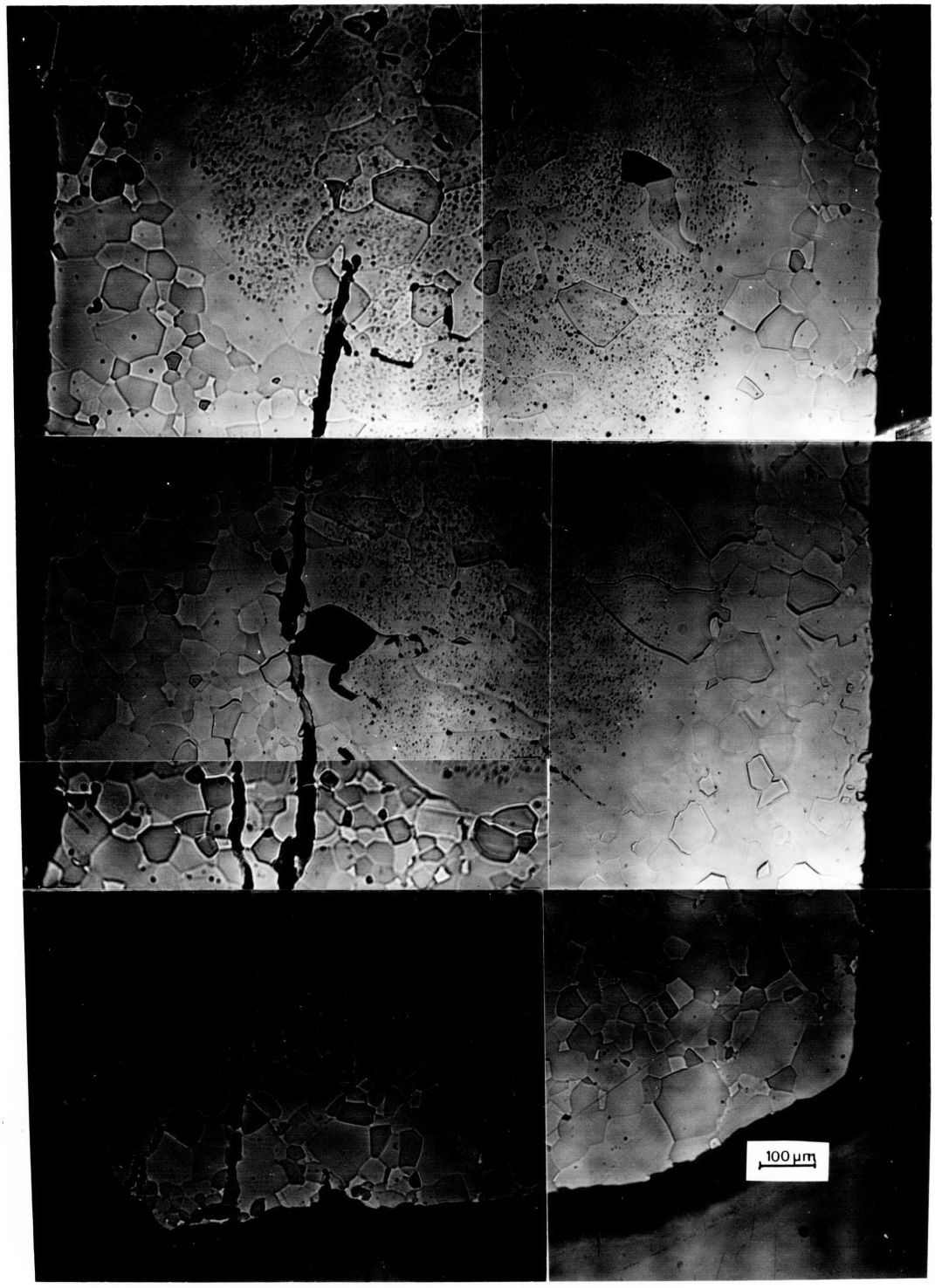

Figure 20. REFLECTED LIGHT VIEW OF THE REGION IN FIG 19

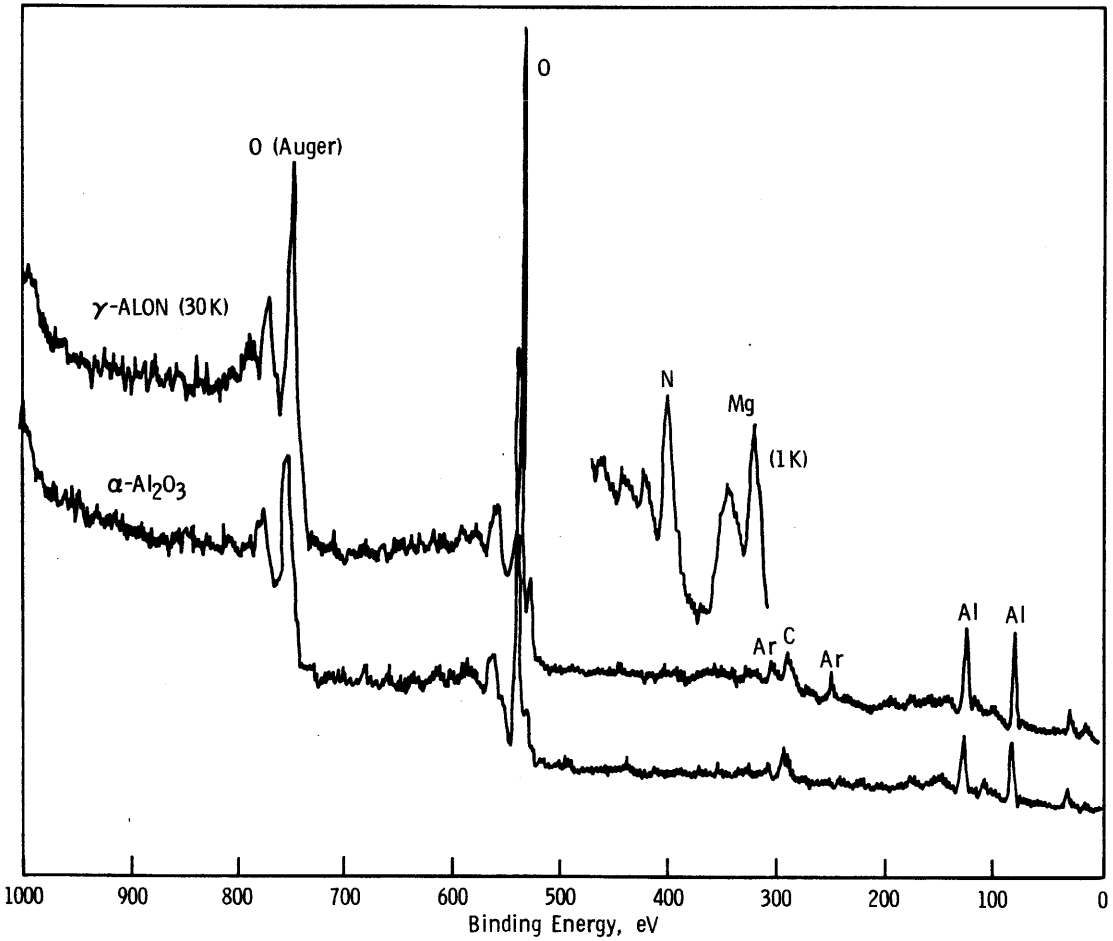

Figure 21. XPS SURVEY SCANS OF γ-ALON AND α-Al_2O_3

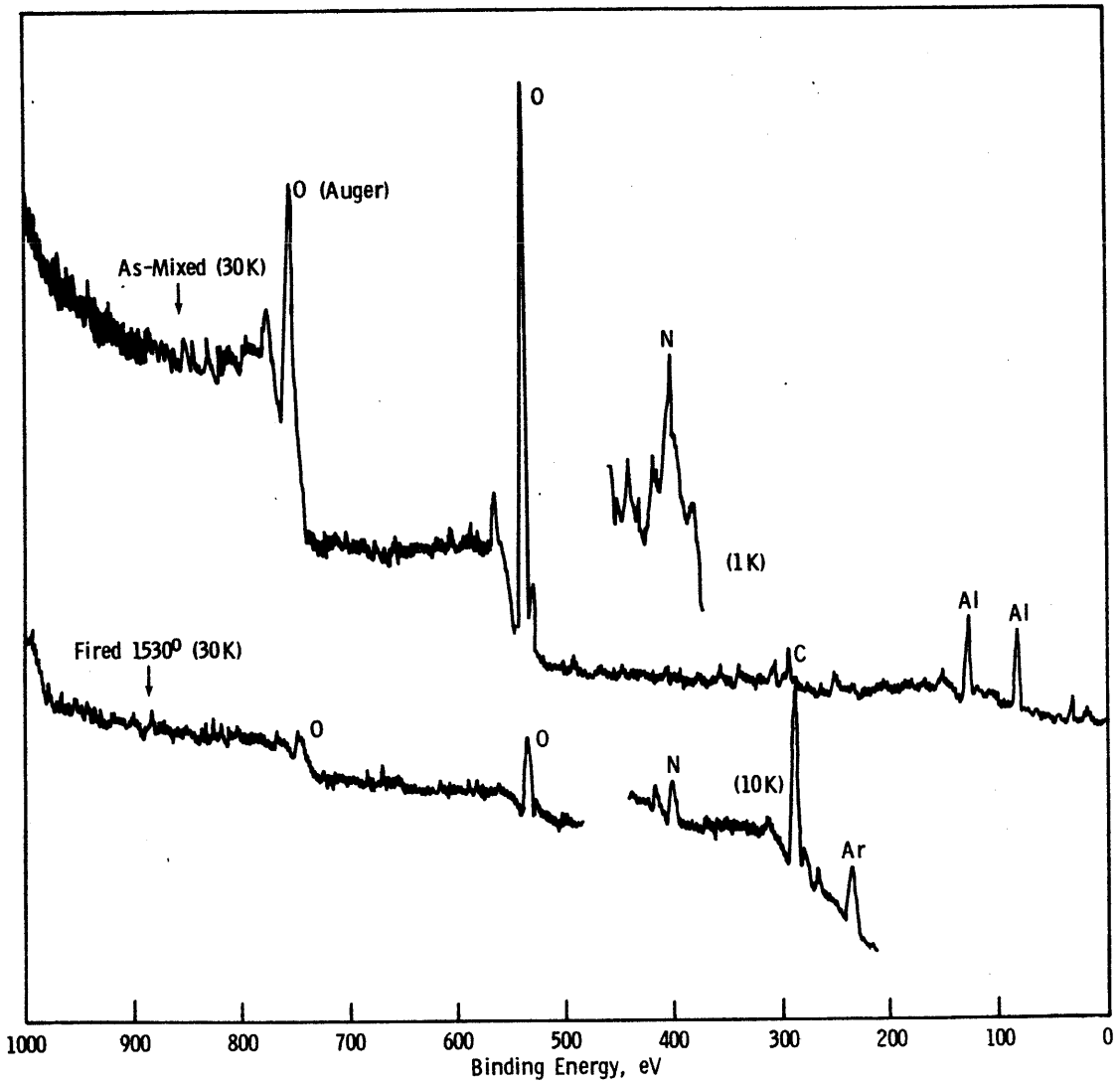

Figure 22. XPS SURVEY SCAN OF 35.7 POWDER MIXTURE

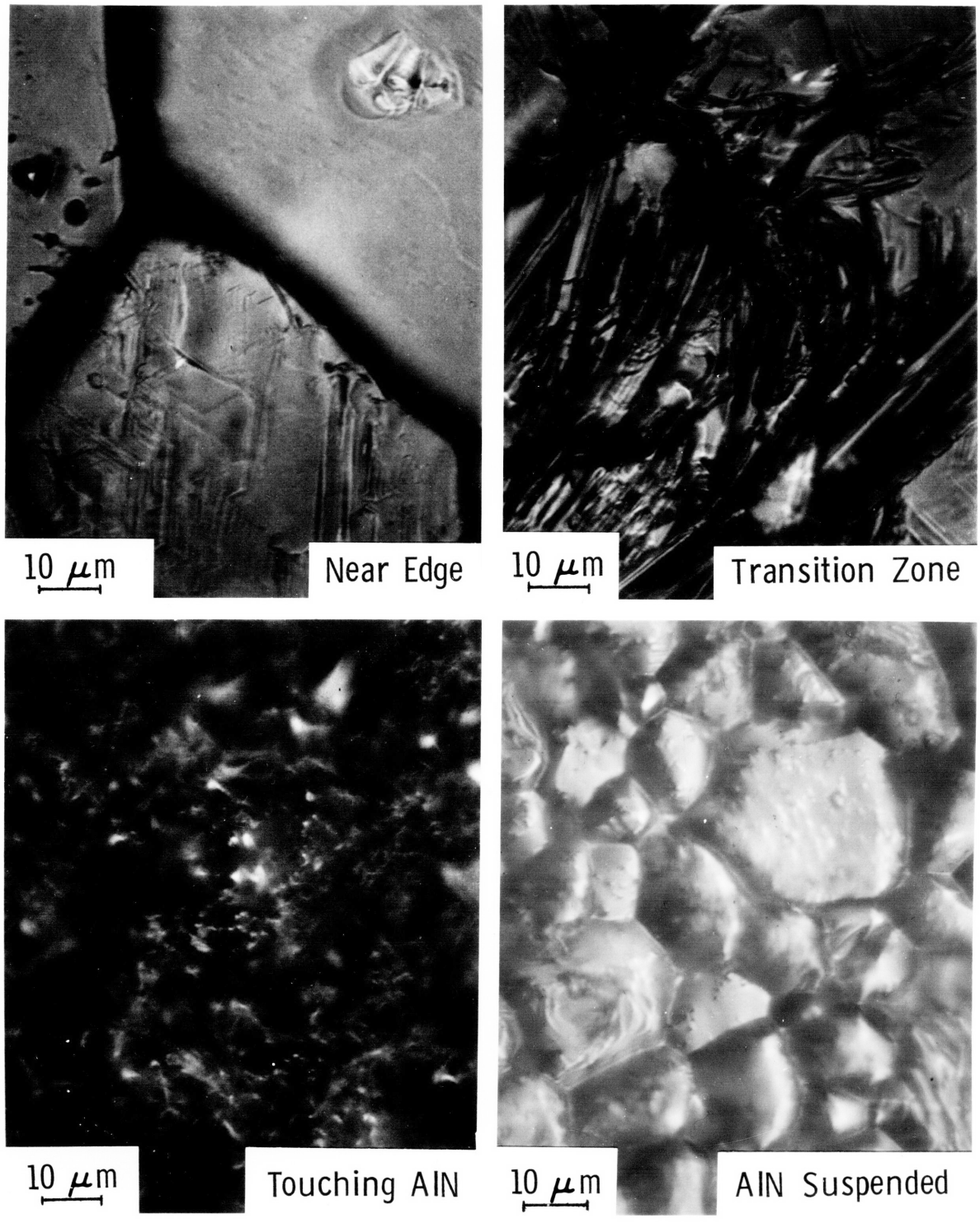

Figure 25. SURFACE OF α-Al_2O_3 PELLETS FIRED IN ARGON AT 1800°C

Table 8. AlN + γ-Al_2O_3 POWDER MIXTURE DATA

Sample	Mole % AlN	Temp. °C	Time at Temp. (hr)	Atmosphere	Furnace	Bulk Density (g/cc)	% γ-ALON	% Weight Loss
161-T	30	1530	1	N_2	Carbon		0	-1.65
176-B	30	1605	0.5	N_2	Carbon		0	-1.88
175-B	30	1605	1	N_2	Carbon		0	-2.09
174-B	30	1605	2	N_2	Carbon		0	-1.98
163-T	30	1745	0.5	N_2	Carbon		80	-2.01
159-T	30	1745	1	N_2	Carbon	2.13	88	-1.57
7	30	1685	1	Ar	Carbon	2.28	89	-2.47
161-M	35.7	1530	1	N_2	Carbon		0	-1.60
175-M	35.7	1605	1	N_2	Carbon		0	-2.11
159-M	35.7	1775	1	N_2	Carbon		80	-1.44
8	30	1800	1	N_2	Ref. Met.	2.69	97	-2.30
9	30	1800	1	Ar	Ref. Met.	2.85	95	-4.16
10	30	1650	1	N_2	Ref. Met.		15	-2.26
11	30	1650	1	Ar	Ref. Met.		5	-2.73

Table 9. DIFFUSION COUPLE DATA

Sample	Temp. °C	Atmosphere	Furnace	AlN Pellet Surface Phase* AlN	α Al_2O_3	γ ALON	% Weight Change	α-Al_2O_3 Pellet Surface Phase* α Al_2O_3	γ ALON	% Weight Change	Remarks
2	1715	N_2	CAR	-	-	-	-	90	10	-2.70	γ-Al_2O_3
3	1715	N_2	CAR	-	-	-	-	80 100†	20 -	-4.56	
5	1715	Ar	CAR	-	-	-	-	100	-	-2.31	
19	1650	N_2	RM	-	-	-	-	100	-	-1.78	
18	1650	Ar	RM	95	5	-	-1.69	-	-	-	
1	1715	N_2	CAR	80†	-	20†	-	100†	-	-	γ-Al_2O_3
4	1905	N_2	CAR	60	-	40	-2.79	(?)	90	-4.00	γ-Al_2O_3
6	1715	Ar	CAR	30	-	70	-2.38	50	50	-2.52	
12	1650	N_2	RM	95	5	-	-0.70	97	3	-2.22	
16	1650	Ar	RM	95	5	-	-1.57	100	-	-1.77	
17	1650	Ar	RM	92	5	3	-1.72	100	-	-1.77	AlN Suspended
20	1800	Ar	RM	100	-	-	-24.24	100	-	-4.06	AlN Suspended

Note: CAR = Carbon; RM = Refractory Metal

*Semiquantitative
†Bulk Phase

Table 10. ELEMENTAL RATIOS FROM XPS SURVEY SCANS

	Ratio	Data	Theory
α-Al_2O_3	O/Al	6.8/1	8.6/1
γ-ALON	O/N	109/1	9/1
35.7 (As-mixed)	O/N	90/1	9/1
35.7 (1530°C)	O/N	6/1	9/1

ASF Values - O = 0.63, N = 0.38, Al = 0.11
Mg = 3.65

Table 11. BINDING ENERGY DATA FROM XPS HIGH RESOLUTION SCANS

	O(1S)ev	O(Auger)ev	α	Al(2P)ev	α
α-Al_2O_3	538.0	752.6	214.6	80.9	671.7
γ-ALON	536.5	751.3	214.8	79.7	671.6
Unfired Mix	537.5	752.4	214.9	80.5	671.9

α = Auger Parameter
α = Photoelectron Binding Energy - Auger Binding Energy for Oxygen

VI. Thermodynamics

In order to better understand the previous results a thermodynamic evaluation was conducted. This evaluation centered on two topics: (1) calculating the equilibrium partial pressures of the important vapor species over AlN and Al_2O_3, and (2) calculating the free energy of reaction ($\Delta G°$) for several processes known to produce γ-ALON.

The thermodynamic data for all chemical species, except γ-ALON, were obtained from JANAF Tables (66). The information for γ-ALON was taken from the previous studies of Dorner(32,33) and Kaufman (34).

VI.1 αAl_2O_3 Vapor Species

As mentioned by Collongues (42) α-Al_2O_3 is not stable in the presence of a reducing agent. This instability may increase the partial pressures of the equilibrium vapor species over αAl_2O_3. Studies by various investigators (67-70), using mass spectrometers, have observed different gaseous species upon the vaporization of alumina in reducing vs neutral conditions. There is general agreement that for reducing conditions $Al_2O_{(g)}$ and $Al_{(g)}$ are the dominant species whereas $Al_{(g)}$ and $O_{(g)}$ are dominant in neutral or oxidizing conditions. Brewer(67) and Yanagida (68) have found the volatility of Al_2O_3 in the presence of aluminum to be several orders of magnitude greater than for pure Al_2O_3.

Figure 23 shows the calculated equilibrium vapor pressures as a function of temperature for Al_2O_3 under various

reducing conditions. In neutral conditions the important reaction is:

$$Al_2O_{3(s)} = 2Al_{(g)} + 3O_{(g)} \quad ,$$

while for reducing conditions $Al_2O_{(g)}$ becomes important due to the reaction

$$2Al_{(g)} + O_{(g)} = Al_2O_{(g)} \quad .$$

These two reactions account for the major vapor species of Al_2O_3. As shown in Fig. 23, without the presence of a reducing agent, both equations have very low equilibrium vapor pressures (10^{-6} to 10^{-9} atm) in the temperature range of interest (1600°C to 2000°C). When αAl_2O_3 is in contact with aluminum or carbon the vapor pressure of $Al_2O_{(g)}$ increases to $10^{-0.5}$ and $10^{-2.5}$ over the same temperature range. These reducing agents have increased the vapor pressures by five orders of magnitude when the following reactions are considered:

$$Al_2O_{3(s)} + 2C_{(s)} = Al_2O_{(g)} + 2CO_{(g)}$$

$$Al_2O_{3(s)} + 4Al_{(l)} = 3Al_2O_{(g)}$$

Since a majority of the work was performed in a graphite furnace, the equilibrium vapor pressure for carbon vapor over carbon was calculated and is also shown in Fig. 23. This carbon vapor is in contact with the Al_2O_3 sample and can react with it by the equation

$$Al_2O_{3(s)} + 2C_{(g)} = Al_2O_{(g)} + 2CO_{(g)}$$

The vapor pressures for the products of this reaction, using the calculated equilibrium vapor pressure for carbon, are also shown in Fig. 24. The influence of carbon vapor can increase the equilibrium partial pressures of $Al_2O_{(g)}$ and $CO_{(g)}$ to 100 atm.

All the above calculations give values for equilibrium vapor pressures, these values would not be obtained in this study because an open system with flowing gases was used. This evaluation does however give insight into the effects reducing agents can have on Al_2O_3 vaporization since the free energy changes for the reduction reactions are larger than for neutral reactions. This vaporization will be very influential in understanding the weight losses and microstructural development of samples.

VI.2 AlN vaporization

For AlN there are only two known vaporization reactions:

$$AlN_{(s)} = Al_{(g)} + \frac{1}{2} N_{2(g)}$$

$$AlN_{(s)} = AlN_{(v)}$$

Schissel and Williams (71) have found only $Al_{(g)}$ and $N_{2(g)}$ present as vapor species over AlN. Using JANAF table information the vapor pressures from both of these reactions were calculated and are shown (dashed lines) in Fig. 23. The reaction producing $AlN_{(v)}$ is negligible compared to that producing $Al_{(g)}$ and $N_{2(g)}$ which has vapor pressures five orders of

magnitude larger, therefore, this latter reaction is strongly influenced by the presence of nitrogen as the firing atmosphere.

VI.3 γ-ALON

IV.3.1. Free energy of formation ($\Delta G°_f$)

The free energy of formation for γ-ALON can be calculated from the data of Dorner et al and Kaufman. These authors use the composition $A\ell_7O_9N$ (25 m/o AℓN) for γ-ALON which occurs outside the solid solution region as determined by McCauley and Corbin (Fig. 2) but inside the limits as reported by Lejus (Fig. 1). Since the limits of γ-ALON solid solution have not been accurately determined, this composition will be used in the thermodynamic calculations below.

Table 12 lists the values of $\Delta G°_f$ for γ-ALON at different temperatures as evaluated from Dorner and Kaufman data. Dorner listed $\Delta H°_f$ and $-\Delta S°_f$ values for γ-ALON which were inserted into the equation:

$$\Delta G°_{f(ALON)} = \Delta H°_{f(ALON)} - T\Delta S°_{f(ALON)}$$

to solve for the free energy of formation of γ-ALON. Kaufman's data was given as the free energy of reaction ($\Delta G°$) to form γ-ALON from αAl_2O_3 and AℓN. Using his information and $\Delta G°_f$ for $Al_2O_{3(s)}$ and $A\ell N_{(s)}$ as listed in the JANAF tables, the $\Delta G°_f$ for γ-ALON is given by the equation:

$$\Delta G°_{f(ALON)} = \Delta G° + 3G°_{f(\alpha Al_2O_3)} + G°_{f(A\ell N)} \quad .$$

The values calculated from the two sets of data do not

agree. They are similar near 1900°K (Table 12) but at other temperatures the differences become large. The reasons for these differences are due to the assumptions used in their determinations. Dorner used the eutectoid decomposition of γ-ALON into αAl_2O_3 and AℓN(1600°C) from the results of Lejus (Fig. 1) and assumed a small positive value (1 Joule/°K gram atom) for the entropy of formation from α-Al_2O_3 and AℓN. Kaufman calculated the free energy of reaction by using lattice stability, solution and compound phase parameters which were selected from observed thermochemical properties and phase diagrams. Even though the differences in $\Delta G°_f$ between the authors appear to be small, they are extremely influential in determining the stability of γ-ALON at low temperatures and its melting behavior. As mentioned in the literature review, these authors obtained different phase diagrams from their calculations. Since Dorner uses the eutectoid in his derivation, his results show γ-ALON unstable below 1600°C. On the other hand, Kaufman does not use the eutectoid so his results show γ-ALON stable down to room temperature.

IV.3.2 Free energies of Reaction ($\Delta G°$)

Using the $\Delta G°_f$ values for γ-ALON listed in Table 12 and JANAF table data, the free energies of reaction ($\Delta G°$) for various γ-ALON formation reactions were calculated. Of special interest are $\Delta G°$ values for equations known to form γ-ALON as listed in Table 5. Some of these equations are

balanced with calculated $\Delta G°$ values at 1700°K and 2300°K listed in Table 13; several are also plotted in Fig. 24.

(a) Al_2O_3 + AlN Reaction. As shown in FIg. 24, there is a significant difference between using Dorner or Kaufman data. Using Kaufman's values the $\Delta G°$ for this reaction is always negative, thus γ-ALON is stable at low temperatures. Dorner, however, has the $\Delta G°$ become positive below 1873°K (1600°C) to agree with the Lejus eutectoid. Silvestri's (48) studies which formed γ-ALON at 900°C disprove this eutectoid. It appears Kaufman's data are more representative of γ-ALON stability.

(b) Al_2O_3 + C + N_2 gas. The thermodynamic evaluation of this reaction shows above 1950°K (1677°C) γ-ALON will form when graphite solid is used. This temperature is nearly equivalent for both Dorner and Kaufman because in this temperature range their $\Delta G°_f$ values are nearly equivalent. This reaction was also thermodynamically investigated by Worrell (72). His studies involved the formation of aluminum carbide by the reaction:

$$2Al_2O_{3(s)} + 3C_{(s)} = AL_4C_{3(s)} + 3O_{2(g)}$$

It is interesting to note when this reaction is carried out in nitrogen either an oxy-nitride or nitride forms. It appears that γ-ALON is more easily formed than Al_4C_3.

Since carbon vapor has a large influence on the equilibrium partial pressures over Al_2O_3 and samples fired in a

graphite furnace are exposed to these vapors, equation 3 in Table 13 was evaluated. This reaction has a large $\Delta G°$ and, therefore, a large driving force, even at 1700°K. The importance of this reaction only occurs at higher temperatures $\gtrsim$ 2100°K because below this the partial pressure of $C_{(v)}$ over $C_{(s)}$, as previously determined (Fig. 23), is less than 10^{-10} ATM. In other words, the reaction occurs when carbon vapor is present but the vapor pressure is too low at low temperatures.

(c) $Al_2O_3 + NH_3$ Reaction. Collongues (43) has previously found this reaction to produce AlN at ~1000°C and if heated above 1650°C γ-ALON results. From the thermodynamic evaluation in Table 13 this reaction should not be possible at such a low temperature. As shown in Fig. 24 this reaction will only occur near 2450°K (for Dorner) which is about 25° above the melting point of γ-ALON. Since Collongues has seen the reaction occur, there must be another important factor which has not been entered into my thermodynamic evaluation. Several possibilities include: the importance of an H_2 atmosphere in his studies, or if free carbon or aluminum was present they may enhance the reaction as they enhance the vaporization.

(d) AL $Cl_3 + NH_3 + CO_2$ Reaction. This reaction was used by Silvestri (48) to vapor deposit γ-ALON on silicon. As shown in Table 13 this reaction has a large negative $\Delta G°$ value, with a slope of $\Delta G°$ vs temperature opposite that of $\Delta G°_f$. So

as temperature is increased this reaction becomes more favorable while formation from the standard states becomes less favorable.

It appears that reactions which do not involve αAl_2O_3 have a much larger $-\Delta G°$. This may be an indication why reactions involving αAl_2O_3 require such high temperatures for γ-ALON formation.

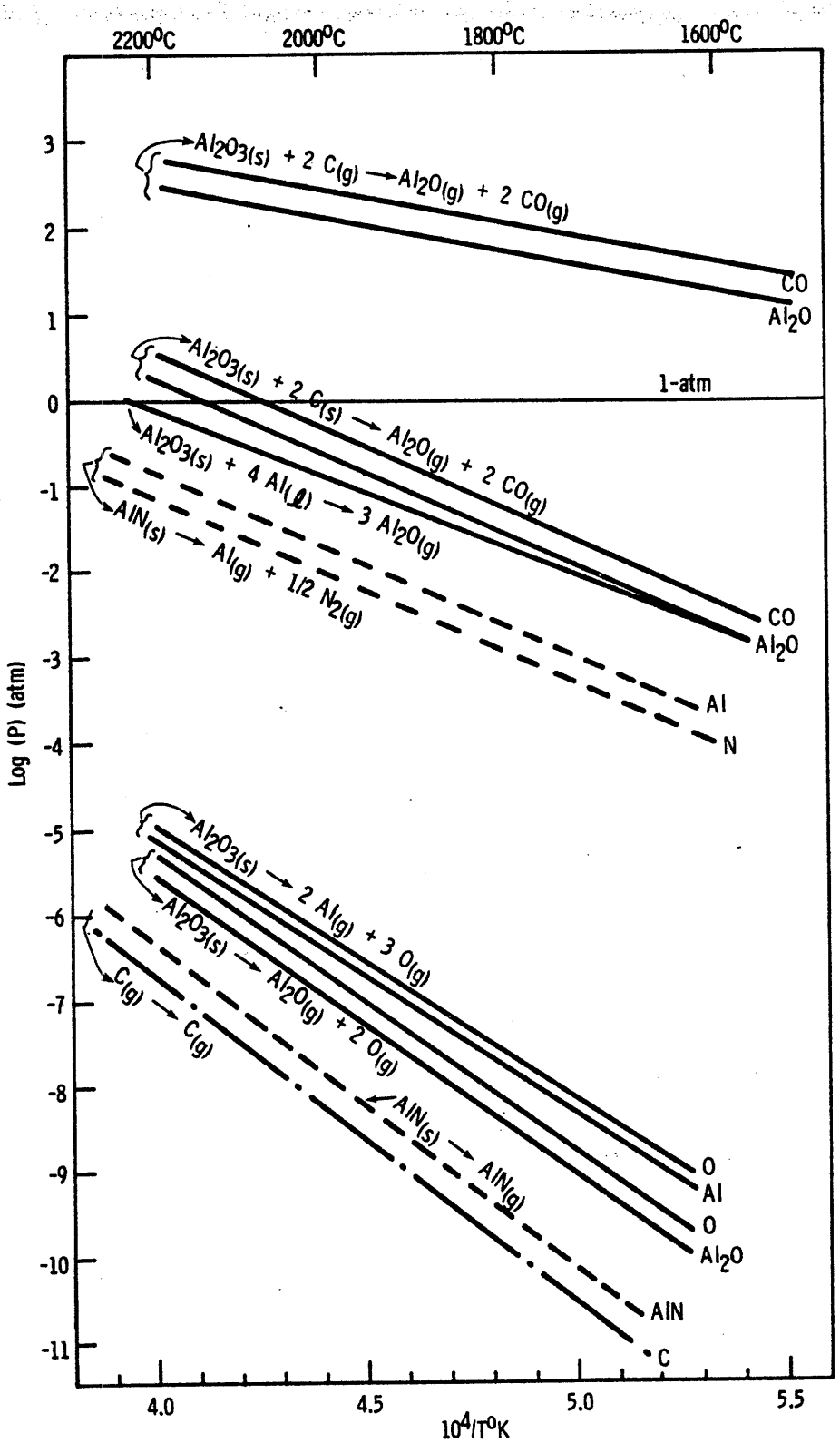

Figure 23. Al_2O_3 AND AlN VAPOR SPECIES

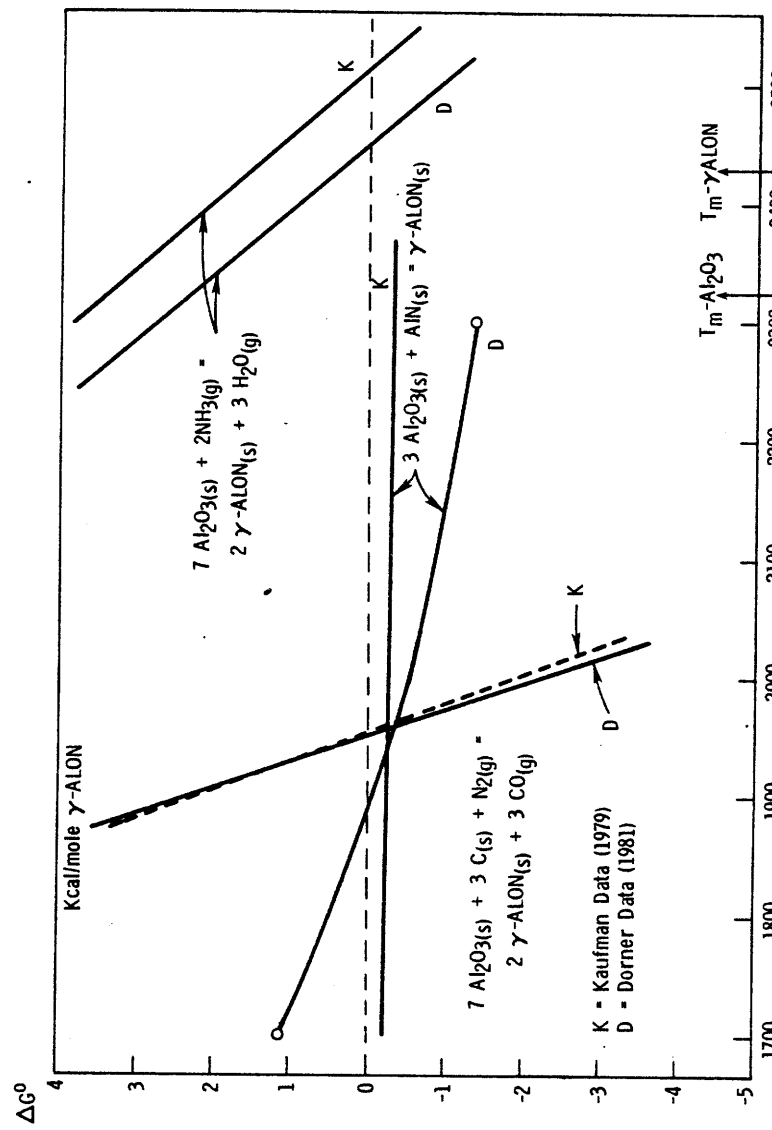

Figure 24. γ-ALON FREE ENERGIES OF REACTION

Table 12. γ-ALON* FREE ENERGY OF FORMATION (ΔG^0_f)

		Kcal mole^{-1} γ-ALON		
T^0K	T^0C	Dorner	Kaufman	Δ
1700	1427	-841.905	-843.242	-1.337
1900	1627	-791.497	-791.667	-0.170
2100	1827	-741.090	-740.455	+0.635
2300	2027	-690.683	-689.568	+1.115
2500	2227	-640.276	-638.998	+1.278

*7 $Al_{(\ell)}$ + 9/2 O_2 + 1/2 N_2 = Al_7O_9N (25 m/o AlN)

Table 13. γ-ALON FREE ENERGIES OF REACTION

		ΔG^0 Kcal/mole	
		1700^0K	2300^0K
	Data	(1427^0C)	(2027^0C)
$3\ Al_2O_{3(s)} + AlN_{(s)} = Al_7O_9N_{(s)}$	D	+1.11	-1.38
	K	-0.23	-0.27
$7\ Al_2O_{3(s)} + 3\ C_{(s)} + N_{2(g)} = 2\ Al_7O_9N_{(s)} + 3\ CO_{(g)}$	D	+11.77	-15.10
	K	+10.43	-13.99
$7\ Al_2O_{3(s)} + 3\ C_{(g)} + N_{2(g)} = 2\ Al_7O_9N_{(s)} + 3\ CO_{(g)}$	D	-148.96	-142.06
	K	-150.30	-140.94
$7\ Al_2O_{3(s)} + 2\ NH_3 = 2\ Al_7O_9N_{(s)} + 3\ H_2O_{(g)}$	D	+15.93	+2.71
	K	+14.59	+3.83
$7\ AlCl_{3(g)} + 9\ CO_{2(g)} + 7\ NH_{3(g)} =$	D	-503.28	-663.68
$Al_7O_9N_{(s)} + 21\ HCl_{(g)} + 9\ CO_{(g)} + 3\ N_{2(g)}$	K	-504.62	-662.57
$7\ Al_{(\ell)} + 9/2\ O_{2(g)} + 1/2\ N_{2(g)} = Al_7O_9N\ (\Delta G^0_f)$	D	-841.91	-640.28
	K	-843.24	-638.998

Note: D = Dorner Data (1981)
K = Kaufman Data (1979)

Table 14. Vaporization Reactions

		ΔG° Kcal/mole	
		1900°k (1627° C)	2300°k (2027° C)
1.	$Al N_{(s)} = Al_{(g)} + \frac{1}{2} N_{2(g)}$	+ 47.84	+ 26.53
2.	$Al N_{(s)} = Al N_{(g)}$	+ 96.73	+ 80.33
3.	$Al_2O_{3(s)} = 2Al_{(g)} + 3O_{(g)}$	+ 391.64	+321.40
4.	$Al_2O_{3(s)} = Al_2O_{(g)} + 2O_{(g)}$	+ 253.82	+206.90
5.	$Al_2O_{3(s)} + 2C_{(s)} = Al_2O_{(g)} + 2CO_{(g)}$	+ 59.77	+ 9.71
6.	$Al_2O_{3(s)} + 2C_{(g)} = Al_2O_{(g)} + 2CO_{(g)}$	- 139.50	-159.57
7.	$Al_2O_{3(s)} + 4Al_{(l)} = 3Al_2O_{(g)}$	+ 66.88	+ 25.26
8.	$Al_2O_{3(s)} + 4Al_{(g)} = 3Al_2O_{(g)}$	- 21.83	- 22.11
9.	$Al_2O_{3(s)} + 2W_{(g)} = Al_2O_{(g)} + 2WO_{(g)}$	+ 28.37	+ 5.56
10.	$C_{(s)} = C_{(g)}$	+ 99.63	+ 84.64
11.	$W_{(s)} = W_{(g)}$	+ 137.28	+122.77
12.	$Al_{(l)} = Al_{(g)}$	+ 22.18	+ 11.84

VII. Discussion

The analysis of experimental results will utilize thermodynamic information on Al_2O_3, AlN, and γ-ALON. Weight losses, material transport and γ-ALON reactions will be used for relating the experimental and thermodynamic data.

The majority of these studies were done in the carbon induction furnace or the tungsten resistance furnace. Four furnace conditions were generated by using nitrogen or argon atmospheres in these furnaces. Equations 6 and 9 of Table 14 indicate that the presence of carbon vapor is very influential in reducing Al_2O_3 and enhancing its vaporization while tungsten vapor is not. This indicates that the furnace used will have a significant influence on the stability of Al_2O_3. Equation 1 in Table 14 shows that nitrogen suppresses the decomposition of AlN while argon will enhance it. Using this information the relative stabilities of AlN and Al_2O_3 can be altered by modifying the firing conditions. The four furnace conditions used were:

(a) carbon + nitrogen; Al_2O_3 unstable, AlN stable

(b) carbon + argon; Al_2O_3 unstable, AlN unstable

(c) tungsten + nitrogen; Al_2O_3 stable, AlN stable

(d) tungsten + argon; Al_2O_3 stable, AlN unstable

These four configurations are also influenced by the presence of aluminum vapor which can also enhance Al_2O_3 vaporization (Eq. 8, Table 14). The

reaction becomes important when AlN is in contact with Al_2O_3 in argon, because Al gasis produced from the decomposition of AlN.

VII.1. Weight Loss

The weight losses of both the diffusion couples and powder mixtures can be explained by three different mechanisms: (a) volatile loss, (b) vaporization reactions, and (c) gas-solid reactions.

VII.1.1 Volatile Loss

A substantial part of the weight loss in all samples is due to volatile loss (esp. H_2O) upon heating. For identical material the percent weight change should be unaffected by different furnace conditions, temperatures, or time. Weight loss due to this cause generally occurs at temperatures well below 1000°C.

Variations in surface area between powders will generate differences in percent weight loss due to the adsorbtion of volatiles on the surface. This is illustrated by the percent weight loss of the two different AlN powders (-24.24% vs -9.82%) and the two Al_2O_3 powders (-4.56% vs -2.20%) when fired under identical conditions.

VII.1.2 Vaporization Reactions

The important vaporization reactions are listed in Table 14; some of their equilibrium vapor pressures are calculated and plotted in Figure 23. The majority of these

equations have already been discussed in the section on thermodynamics in this work.

For equilibrium partial pressures to be a source of information on weight losses, ideally equilibrium in a closed system should be obtained. However, this work was carried out in an open system with flowing gases. As discussed by Kingery et al (73) the evaporation rate depends on the thermodynamic driving forces, surface reaction kinetics, conditions of the reaction surface, and ambient atmosphere. If evaporation is not controlled by the interface reaction rate, it can be evaluated by the Knudsen equation. For high partial pressures this assumption is generally valid.

$$\frac{\partial n_i}{\partial t} = \frac{A\, P_i\, \alpha_i}{\sqrt{2\pi\, M_i RT}}$$

$\frac{\partial n_i}{\partial t}$ = loss of i^{th} species in # moles per unit area per unit time

A = sample area

P_i = pressure of i^{th} species above sample

M_i = molecular mass of i^{th} species

α_i = evaporation coefficient

R = gas constant

T = temperature

Identical samples under different atmospheric conditions changes P_i, and will cause different evaporation rates. Thus the weight losses will change.

The data from diffusion couple samples and powder mixture samples will be discussed separately. The weight loss data will be compared and explained using thermodynamic information on vaporization. Percent weight loss values are given in parentheses.

(a) Diffusion Couple Samples

The results show AℓN has a higher weight loss in argon than nitrogen (-.70 vs -1.57). This occurs because the nitrogen atmosphere suppresses AℓN vaporization. Alumina heated in the tungsten furnace has the same weight loss when fired in argon or nitrogen (-1.77) because under these furnace conditions Al_2O_3 is stable. It was expected that Al_2O_3 stability will be affected by the presence of carbon but no conclusive data has been obtained.

The decomposition of AℓN produces Aℓ vapor which can increase the weight loss of Al_2O_3 by equation 8 in Table 14. This reaction can be seen by the different weight losses when Al_2O_3 is fired alone and in contact with AℓN in argon at 1715°C (-2.31 vs -2.52), and at 1650° in nitrogen (-1.78 vs -2.22). This reaction also accounts for the large vaporization of the Al_2O_3 surface in contact with AℓN (1800°C, in argon) as shown in Fig. 25. This dramatic vaporization does not appear at 1650°C and is probably due to the much lower Aℓ vapor pressure at this temperature.

In the diffusion couple studies it is possible that vapor produced in one pellet may condense on the other pellet. This transport can influence the weight

changes of each sample but has only been seen at high (~1700°C) temperatures. This transport method will be further considered in the section on γ-ALON reactions.

(b) Powder Mixture Samples

The powder mixture contains approximately 85 weight percent γ-Al_2O_3 and 15 weight percent AℓN. Because of the disproportionate amount of Al_2O_3 present it will have a large influence on the percent weight loss of these samples.

The weight loss in the tungsten furnace with nitrogen remains constant as temperature increases since both Al_2O_3 and AℓN are stable for this condition. When using argon in the same furnace the higher temperatures produce a large weight loss (-2.73 vs -4.16) due to increased AℓN vaporization. Samples heated in argon have a higher weight loss than heating in nitrogen for the same reason.

In these samples as in the diffusion couple samples Aℓ vapor from AℓN decomposition must be reacting with the Al_2O_3 powder.

VII.1.3 Gas-Solid Reactions

A true solid state reaction will not result in any weight changes. However, in the presence of reactive vapors (Aℓ, C, N) Al_2O_3 can form γ-ALON with a weight loss, such as from the reaction:

$$23Al_2O_3 + 15C_{(g)} + 5N_{2(g)} = 2Al_{23}O_{27}N_5 + 15CO_{(g)} \qquad \begin{matrix}\%\ wt\ \Delta \\ (-4.26)\end{matrix}$$

When Aℓ vapor is substituted for carbon vapor in the above

reaction an identical weight change will occur. The given reaction will not occur in argon or the tungsten furnace. This reaction explains the larger weight loss when Al_2O_3 is heated in nitrogen instead of argon in the carbon furnace (-4.56 vs -2.31). If this reaction occurs using Aℓ vapor from AℓN decomposition, the analysis becomes more complex, because both Aℓ vapor and N_2 gas are produced from decomposition. A nitrogen atmosphere will suppress the decomposition and therefore influence the availability of Aℓ vapor. Several powder mixture samples show smaller weight losses when heated at longer times or higher temperatures in the carbon furnace with nitrogen but not the tungsten furnace. This phenomenon occurs only above the reaction temperature to form γ-ALON from AℓN + Al_2O_3. It is possible that the nitrogen atmosphere starts to react with the samples without simultaneous oxygen loss. This could explain the observed weight changes.

VII.2 Material Transport

Yamaguchi and Tokuda (74) consider two kinds of transport in a powder mixture: material transport of one reactant onto the other, and diffusional transport into the lattice. The difference between these two can be seen in forming Zn Al_2O_4 from ZnO and Al_2O_3 powders. ZnO is known to coat the Al_2O_3 particles by vapor phase transport (75), yet the reaction occurs by the counter diffusion of Aℓ and Zn cations

through the oxygen lattice (74). Since both mechanisms of transport are very different, they will be discussed separately for γ-ALON.

V.2.1 Powder Reactions

Many powder reaction kinetics follow a model proposed by Carter (75). This model was developed for gas-solid type reactions but can also be applied to powder mixtures. It applies when either high surface diffusion or high vapor pressures allow rapid coating of one component by the other. Thus, when the kinetics of this model are followed, the reaction is more representative of a gas-solid reaction than a solid-solid reaction. As discussed previously, both AlN and Al_2O_3 can have high vapor pressures—therefore the γ-ALON reaction could be expected to follow this model.

X-ray photoelectron spectroscopy (XPS) analysis was used in place of kinetic studies to determine whether vapor transport and surface diffusion are important in γ-ALON reactions. Using XPS, changes in the surface chemistry of the particles prior to reaction were evaluated. As shown in Table 10 the oxygen/nitrogen ratio between the 35.7m/o sample prior and after heating (1530°C) changes dramatically from 90/1 to 6/1. The latter value shows more nitrogen present on the surface than the mixed composition would predict. These data are consistent with the following mechanism. Initially the AlN powder is covered with αAl_2O_3 from ball milling, hence the 90/1 ratio. When heated to 1530°C in the carbon furnace,

Al_2O_3 vaporization will occur, remove the oxide layer from AlN, and decreased the O/N ratio. Surface diffusion or evaporation condensation of AlN on Al_2O_3 surfaces could lead to larger than predicted values of N_2 at the surface. Another explanation for the increased nitrogen content is due to the reaction between αAl_2O_3, carbon, and nitrogen to form a nitrided surface. This reaction, however, is not thermodynamically possible below 1690°C. To properly analyze this effect, samples should be made to eliminate the oxide layer on AlN. Conceivably, adjusting furnace conditions could allow changes to be made in which species (AlN or Al_2O_3) coats the other.

X-ray diffraction results of diffusion couple surfaces indicated no transfer of Al_2O_3 or AlN between pellets below 1600°C. This tends to contradict the XPS results. But, X-ray diffraction is not a surface sensitive technique and therefore would not detect a thin surface layer nor can it detect a noncrystalline phase. XPS does not have these limitations and could readily detect a thin noncrystalline surface layer.

VII.2.2 Sintering

Sintering in the Al_2O_3 + AlN powder mixtures can be seen by comparing the microstructures of unfired (Fig. 13) to fired samples (Fig. 15-Fig. 18). The driving force for this phenomena is the lowering of the surface free energy of the system by decreasing the surface area. Sinter-

ing may or may not produce densification—these two possibilities will be discussed separately for γ-ALON fabrication.

(a) No Densification

When surface area reduction occurs by evaporation/condensation, no densification of the sample results. This method of sintering is important for materials with vapor pressures above 10^{-4} to 10^{-5} atm. This mechanism operates by transporting material from regions of higher vapor pressures (small particles, positive radius of curvatures) to lower pressures (large particles, negative radius of curvatures). As shown in Fig. 23, several vapor species of AℓN and Al_2O_3 can achieve high vapor pressures. Considering this, evaporation and condensation must be important for the microstructural development of the AℓN + Al_2O_3 powder mixture.

Figure 13 shows a fracture surface of the original as-mixed powder pellet. As previously described, heating causes the sample to take on a coarser appearance (16a,17a) at 1530°C. This has occurred solely by the elimination of fines in the original compact. This finer fraction evaporated and then condensed on the larger particles. In the initial powder mixture AℓN particles are smaller than γ-Al_2O_3 (Fig. 10)—therefore, it is conceivable that they have coated the Al_2O_3 particles. The previous XPS results tend to substantiate this. The rectangular shaped γ-Al_2O_3 (Fig. 10a,b) particles have been rounded during this sintering process.

Besides particle coarsening, this mechanism can bond the particles together by neck growth. This occurs due to differences in vapor pressures between the point of contact (neck area) and the particle surface. This bonding is obvious in samples heated at higher temperatures (~1600°C, Fig. 15, 16b). Even at these temperatures the sample only consists of AℓN and αAl_2O_3 since no γ-ALON has formed. Densities were not obtained on these samples, but from the microstructures there does not appear to be any densification.

(b) Densification

As shown in the microstructures of samples heated at higher temperatures (>1650°C), a reduction in porosity and neck growth has occurred (Fig. 16c, 17b, 17c, 18). All of these samples have also started to form γ-ALON. This tends to show a relationship between γ-ALON formation and the initiation of densification. In order for densification to occur, diffusional transport is required. For the reaction to proceed, mass transport is also necessary. Therefore at high temperature (>1650°C) grain boundary and/or lattice diffusion must become important allowing both reaction and densification to proceed simultaneously.

Samples fired at 1800°C show higher densities and more reaction than those fired at 1650°C. When fired in argon, larger particles (more coarsening) occur than in nitrogen even though the densities and % γ-ALON formed are

the same (Fig. 17c, 18d). The coarsening effect is largely due to the instability of AℓN in argon which allows more vapor transport. Both the amount of γ-ALON formed and densities are not affected by the atmosphere used. This shows the bulk diffusional transport method is not affected by these atmospheres.

Samples heated in argon in the tungsten furnace have a finer particle size than those heated in the carbon furnace. This is attributed to both phases (Al_2O_3 and AℓN) being unstable in the carbon furnace with argon. These conditions will produce more vaporization and therefore more particle growth than in the tungsten furnace.

It has been demonstrated that the vapor species which form under different furnace conditions have large influences on the microstructural development of γ-ALON.

VII.3 γ-ALON Reactions

VII.3.1 Reaction Thermodynamics

Table 13 lists several reactions for producing γ-ALON with their respective $\Delta G°$ values at 1700°K and 2300°K. Along with Fig. 23 it shows the solid state reactions involving Al_2O_3 only have negative free energies above 1600°C. This is also the case when the reaction is calculated using ammonia.

If carbon vapor or aluminum vapor (data below) react with Al_2O_3 the free energies of reaction become more favorable.

$$3Al_2O_{3(s)} + A\ell_{(g)} + \frac{1}{2} N_{2(g)} = Al_7O_9N_{(s)}$$

$\Delta G^\circ_{1700°K}$ kcal/mole - 57.49 (Dorner), -58.83 (Kaufman)

$\Delta G^\circ_{2300°K}$ kcal/mole -28.21 (Dorner), -26.79 (Kaufman)

The problem with carbon is it has a very low equilibrium vapor pressure (Fig. 23) which means even though the reaction is favorable it is difficult to obtain carbon vapor. However, as shown in Fig. 23, the vapor pressure of $A\ell_{(g)}$ from AℓN is much larger than for carbon. This makes the reaction involving $A\ell_{(g)}$ to produce γ-ALON very important.

Even considering the vapors described above free energies of reaction when using Al_2O_3 are less favorable than when Al_2O_3 is absent as shown by equations 5 and 6 in Fig. 13. This seems to give strong evidence that the requirement of such high temperatures of reaction when αAl_2O_3 is used is due to its high temperature stability. This material however becomes unstable above ~1600°C in a reducing environment (C, Aℓ, NH_3) which then allows for γ-ALON formation. The stability of α-Al_2O_3 in nonreducing environment explains why no oxy-nitride was fabricated in the high temperature plasma. The nitrogen plasma alone is not reducing enough to unstabilize the αAl_2O_3. A mixture of αAl_2O_3 and a reducing agent fed into the plasma might give favorable results. Vardelle and Besson (65) were able to

produce γ-Al_2O_3 by plasma spraying αAl_2O_3 in nitrogen/hydrogen mixtures. There is a possibility that what they call γ-Al_2O_3 could be γ-ALON since both materials have similar spinel structures which could lead to misinterpretation.

The effect of the Al_2O_3 stability is also assumed to preclude oxynitride formation using Aℓ metal at temperatures up to 1000°C. The aluminum metal has an oxide layer on it which protects the metal particles. As found by Bouriannes, the oxy-nitridation of aluminum in air depends on the gas pressure. At low temperatures, the oxide formation may be assumed to prevent oxy-nitridation. If unoxidized aluminum could be heated in air above some critical temperature (where nitrogen affinity equals oxygen affinity) then the oxynitride may form. Bouriannes also noted that above 1500°C the oxy-nitridation of Aℓ does become spontaneous. This temperature may be a key as to the instability of the surface oxide layer, or the start of sufficiently rapid kinetics.

Comparing the results of Al_2O_3 + C, Al_2O_3 + Aℓ, and Al_2O_3 + AℓN mixtures gives insight as to the effectiveness of carbon and aluminum as reducing agents. The mixture using carbon yields double the amount of γ-ALON than the other mixtures for identical conditions. The other two mixtures give very similar results which is reasonable since the chemistry is the same. It is possible the aluminum metal reacted with nitrogen to form AℓN prior to γ-ALON formation.

VII.3.2 Diffusion

As previously discussed both densification and reaction require diffusional transport of material. This may explain why both methods occur simultaneously for γ-ALON.

The actual diffusion mechanism for this material may be very different from that for typical spinels. As shown for spinel reactions in the systems NiO - Al_2O_3 (76), MgO-Al_2O_3 (77), and ZnO-Al_2O_3 (74), the reaction proceeds by cation counterdiffusion through the spinel layer. If counterdiffusion is important for γ-ALON, it would be counterdiffusion of the anions (oxygen, nitrogen). This type of diffusion would only be expected to occur at very high temperatures. Therefore the requirement of high temperatures to observe γ-ALON reaction may be influenced by this anion diffusion.

VIII. Conclusions

1. General

(a) The free energy of formation as a function of temperature derived for γ-ALON by Kaufman gives more representative results for the stability of γ-ALON in nitrogen than other authors' derivations. This is demonstrated by the fabrication of γ-ALON at 900°C and observed congruent melting.

(b) When α-Al_2O_3 is used as a starting component, temperatures in excess of 1600°C are required for producing γ-ALON.

(c) With αAl_2O_3 in nitrogen at 1650°C carbon vapor facilitates γ-ALON formation.

(d) The development of vapor species are critical for fabricating γ-ALON by reacting Al_2O_3 and AℓN.

(e) A nitrogen atmosphere (~1 atm) suppresses the AℓN decomposition while argon (~1 atm) enhances it.

2. Diffusion Couple

(f) Aluminum vapor, from the decomposition of AℓN, reacts with and increases the weight loss of αAl_2O_3 at and above 1650°C.

(g) At 1800°C and above the interaction between AℓN and Al_2O_3 pellets is attributed to a mutual exchange of oxygen and nitrogen (gases).

(h) At 1900°C in nitrogen there is no apparent interaction between AℓN and Al_2O_3 pellets.

3. Powder Mixtures

(i) When Al_2O_3 + AlN powder mixtures are used to produce γ-ALON, larger weight losses and coarser microstructures occur in argon than in nitrogen.

(j) Al_2O_3 + carbon mixtures in nitrogen at 1650°C produce more γ-ALON than Al_2O_3 + AlN mixtures heated at identical conditions.

IX. Future Work

Since aluminum oxy-nitride spinel (γ-ALON) is a relatively new material very few basic studies have been conducted on it. The list below is an outline for some possible future fundamental studies on γ-ALON:

(a) Determination of the diffusion coefficients for oxygen and nitrogen in γ-ALON

(b) Investigation as to why discontinuous grain growth does not occur in this material

(c) Effects of atmosphere on final stage sintering

(d) Investigation into producing γ-ALON by various processing routes

(e) Importance of twinning on sintering behavior.

APPENDIX I

The methods for calculating powder mixtures to produce single phase γ-ALON are described below.

A. Al_2O_3 + AℓN mixture

$$7\ Al_2O_3 + 3A\ell N = \gamma\text{-ALON (30m/o A}\ell\text{N)}$$

$$30 \text{ mole A}\ell\text{N} \times \frac{40.99\text{g}}{\text{mole A}\ell\text{N}} = 122.97\text{g A}\ell\text{N} \quad \underline{14.697 \text{ w/o A}\ell\text{N}}$$

$$70 \text{ mole } Al_2O_3 \times \frac{101.96\text{g}}{\text{mole } Al_2O_3} = 713.72\text{g } Al_2O_3 \quad \underline{85.303\text{w/o}Al_2O_3}$$

However the Al_2O_3 in the milled AℓN must be factored in. The oxygen content of this powder, after milling and drying, is 5.38 wt % from neutron activation. This is equivalent to having 11.43 weight percent of Al_2O_3 in the prepared AℓN. Therefore to make 100 grams of a γ-ALON (30m/o AℓN) powder mixture requiring 14.697g AℓN and 85.303g Al_2O_3, one must add:

$$14.697\text{g A}\ell\text{N} \times \frac{1\text{g milled A}\ell\text{N}}{.886\text{g A}\ell\text{N}} = 16.588\text{g milled A}\ell\text{N}$$

which contains (16.588-14.697) 1.891g Al_2O_3

to (85.303-1.891) 83.412g Al_2O_3

B. Al_2O_3 + Carbon Mixture

$$17\ Al_2O_3 + 9C + 3N_2 = \gamma\text{-ALON (30m/o A}\ell\text{N)} + 9CO$$

$$17 \text{ moles } Al_2O_3 \times \frac{101.96\text{g}}{\text{mole}} = 1733.32\text{g } Al_2O_3 \quad \underline{94.130 \text{ w/o } Al_2O_3}$$

$$9 \text{ moles C} \times \frac{12.01\text{g}}{\text{mole}} = 108.09\text{g C} \quad \underline{5.870 \text{ w/o C}}$$

C. Al_2O_3 + Aℓ mixture

$$9\ Al_2O_3 + 5A\ell + \frac{5}{2}\ N_2 = \gamma\text{-ALON (35.7 m/o A}\ell\text{N)}$$

$$9\ \text{moles}\ Al_2O_3 \times \frac{101.96g}{\text{mole}} = 917.64g\ Al_2O_3 \qquad 87.183\ \text{w/o}\ Al_2O_3$$

$$5\ \text{moles}\ A\ell \times \frac{26.98g}{\text{mole}} = 134.90g\ A\ell \qquad 12.817\ \text{w/o}\ A\ell$$

APPENDIX II

In order to accurately determine the percentage of γ-ALON which has formed by the reaction of $A\ell N$ and Al_2O_3 powder mixtures, reaction standards were made. The reaction equation used for developing the standard is;

$$5\ A\ell N + 9\ Al_2O_3 = Al_{23}O_{27}N_5$$

Since this is a solid state reaction the mass of material remains constant during reaction. The equation below was used for evaluating the mole percentages of each phase present as the reaction goes to completion, where (x) is the mole fraction of $Al_{23}O_{27}N_5$ formed.

$$5\ A\ell N + 9\ Al_2O_3 \rightarrow (x)\ Al_{23}O_{27}N_5 + (1-x)(5A\ell N + 9Al_2O_3)$$

Knowing the moles of each phase present allows calculating their weight percentages. Using these calculated weight percentages at different stages of reaction several mixtures of $A\ell N$, αAl_2O_3, and γ-ALON were made. These powder mixtures were analyzed by X-ray diffraction using CuK^{α} radiation and a Ni filter. Reaction standard charts were drawn by plotting selected peak height ratios against the weight percentage of γ-ALON in the powder mixture. Best results were obtained by using the highest intensity (I = 100) peaks of $A\ell N$ and α-Al_2O_3 and the peak at 60.73° (2θ, Cuk^{α}) for γ-ALON.

To determine the weight percentage of γ-ALON in fired samples the appropriate ratios were taken and matched with the percent γ-ALON formed from the master chart.

Bibliography

1. H.C. Stumpf, A.S. Russell, J.W. Newsome, and C.M. Tucker Ind. and Eng. Chem., 42, p. 1398, (1950).

2. M.H. Jellinek and I. Fankuchen, Ind. and Eng. Chem., 37, p. 158, (1945).

3. J.E. Blendell and R.L. Coble, J. Am. Ceram. Soc. 65, p. 174, (1982).

4. G. Yamaguchi, J. Electrochem. Soc. Japan (Denki-Kagaka), 14, p. 106, (1946).

5. G. Yamaguchi, J. Ceram. Assoc. Japan (Yogyo-Kyoki-Shi) 55, p. 42 (1947).

6. G. Yamaguchi, Chem. Soc. of Japan, 23, p. 89, (1950).

7. N.E. Filonenko, I.V. Lavrov, O.V. Andreeva, and R.L. Pevzner, Academy of Science of USSR - Proceedings, Chem. Tech. Soc., 115 , p. 41, (1957).

8. Z.L. Vert, M.V. Kamentsev, V.I. Kudryavtsev and M.I. Sokhor, Acad. of Sci. USSR Proceedings, Chem. Tech. Sec. 116, p. 75, (1957).

9. G. Yamaguchi and H. Yanagida, Chem. Soc. of Japan, 32 p. 1264, (1959).

10. T. Sakai and M. Iwata, J. Mater. Sci. 12, p.1959 (1977).

11. T. Sakai, M. Kuriyama, T. Inukai, T. Kizimia, J. Ceram. Assoc. Japan, 86, p. 174, (1978).

12. J.P. Lecompte, J. Jarrige, J. Mexmain, R.J. Brook and F.L. Riley, J. of Mat. Sci. 16, p. 3093, (1981).

13. T. Sakai, J. Am. Ceram. Soc., 69, p. 460, (1978).

14. H.K. Jack, J. Mat. Sci., 11, p. 1135 (1976).

15. H.K. Jack, Phase Diagrams: Materials Science and Technology, Vol. V, Ed. by A.M. Alper, Academic Press, New York, p. 241 (1978).

16. L.J. Gauckler and G. Petzow, Nitrogen Ceramics, Ed. by F.L. Riley, Noordhoff Pub. Co., The Netherlands, p. 41, (1977).

17. N.D. Corbin and J.W. McCauley, Proceedings of "SPIE 25th Annual Int. Tech. Symp. and Exhibit," 24-28 Aug. 1981, San Diego, Cal.

18. T.M. Hartnett, E.A. Maguire, R.L. Gentilman, N.D. Corbin, and J.W. McCauley, submitted to Ceram. Eng. and Sci. Proc.

19. T. Sakai, J. Ceram. Assoc. Japan, 86, p. 125 (1978).

20. I. Adams, T.R. AuCoin, and G.A. Wolff, J. Electrochem. Soc. 109, p. 1050 (1962).

21. G. Long and L.M. Foster, J. Am. Ceram. Soc., 42, p. 255 (1961).

22. S.F. Bartram, G.A. Slack, Acta. Cryst., B-35, p.2281 (1979).

23. P.A. Lefebvre, J.Appl. Cryst., 8, p. 235, (1975).

24. J.W. McCauley, J.Am. Ceram. Soc., 61, p.372, (1978).

25. P. Goursat, P. Goeuriot, M. Billy, Mat. Chem. 1, p. 131, (1976).

26. P. Goursat, M. Billy, P. Goeuriot, J.C. Labbe, J.M.Villechenoux, G. Boult and J. Bardolle, Mat. Chem. 6, p.81 (1981).

27. D. Michel, Rev. Int. Hautes Temper. et Refrac., 9, p.225, (1972).

28. A.M. Lejus, Rev. Hautes Temper. et Refract., 1, p.53 (1964).

29. J.W. McCauley and N.D. Corbin, J.Am. Ceram. Soc., 62, p.476, (1979).

30. J.W. McCauley and N.D. Corbin, Submitted to Nato Advanced Study Inst. on Nitrogen Ceramics, Aug. 1981.

31. J.L. Henry, J.H. Russell and H.J. Kelly, U.S. Dept. of the Interior, Bu. of Mines Rept. No. 7320, Nov. (1969).

32. P. Dorner, L.I. Gauckler, H. Krieg, H.L. Lukas, G.Petzow, and J.Weiss, Calphad, 3, p. 241 (1979).

33. P. Dorner, L.J. Gauckler, H. Krieg, H.L. Lukas, G.Petzow and J.Weiss, J.Mat. Sci., 16, p. 935 (1981).

34. L. Kaufman, Presented at CALPHAD VIII, Stockholm, Sweden (1979).

35. W.D. Kingery, H.K. Bowen, D.R. Uhlmann, Introduction to Ceramics, Second Edition, John Wiley & Sons Inc., p. 62, (1976).

36. R. Kieffer, W. Wruss, B. Willer, Rev. Int. Hautes. Temper. et Refrac., 13, p.97 (1976).

37. N.D. Corbin and J.W. McCauley, Am. Ceram. Soc. Bull., 59, p.373 (1980).

38. W. Rafaniello and I.B. Cutler, J. Am. Ceram. Soc., 64, p.C-128 (1981).

39. M. Ish-Shalom, Am. Ceram. Soc. Bull., 59, p.827 (1980).

40. D. Michel, M. Perez y Jorba, and R. Collongues, C.R.Acad. Sci. Ser. C, 263, p.1366 (1966).

41. R. Collongues, J.C. Gilles, A.M. Lejus, M. Perez y Jorba, et D.Michel, Mat. Res. Bull. 2, p.837 (1967).

42. R. Collongues, F. Colin, J. Thery, D. Michel, and M. Perez y Jorba, Bull. Soc. Fr. Ceram., 77, p.51 (1967).

43. R. Collongues, J.C. Gilles, and A.M. Lejus, Societe Chimique de France, Bulletin p. 2113 (1962).

44. D. Michel and M. Huber, Rev. Int. Hautes. Temper. et Refract., 7, p.145 (1970).

45. R. Bouriannes, Rev. Int. Hautes. Temper et Refract., 10, p.113 (1973).

46. R. Bouriannes, A. Hardy and N. Manson, C.R. Acad. Sci. Ser. C, 274, p.817 (1972).

47. E.A. Irene, U.J. Silvestri, G.R. Woolhouse, J.Electronic Mat., 4, p.409 (1975).

48. U.J. Silvestri, E.A. Irene, S.Zirinsky, and J.D. Kaptsis, J. Electronic Mat., 4, p.429 (1975).

49. F. Grekov, D. Demidov and A. Zykov, Zh. Prikl. Khim. (Leningrad), 57, p.1450 (1978).

50. K. Dreyer, H. Grewe, J. Kolaska, and N. Reiter, Chemical Abstracts, 172316y,93, (1980).

51. H. Tanaka and Y. Yamamoto, Chem. Abs. 111319j, 91 (1979).

52. Z. Nishizawa and I. Shioda, Chem. Abs. 225314e, 92 (1980).

53. P.E. Dotterty and R.S. Davis, J. Appl. Phys. 34, p.619 (1963).

54. W.D. Kingery, H.K. Bowen, D.R. Uhlmann, Introduction to Ceramics, Second Edition, John Wiley & Sons Inc (1976), Chapter 18.

55. N.D. Corbin, "Grain Boundry Phase Identification Using Ultropak Microscopy," to be published.

56. T. Sakai and A. Watanabe, Am. Ceram. Soc. Bull. 58, p.853 (1980).

57. M. Billy, Nitrogen Ceramics, Ed. by F.L. Riley, Noordhoff Publishing Co., The Netherlands, p. 203 (1977).

58. A.M. Lejus, Societe Chimique de France, Bulletin p.2123 (1962).

59. C.G. Pantano, Am. Ceram. Soc. Bull. 60, p.1154 (1981).

60. C.D. Wagner, W.M. Riggs, L.E. Davis, and J.F. Moulder, Handbook of X-ray Photoelectron Spectroscopy, Ed. by G.E. Muilenberg, Perkin-Elmer Corp., Eden Prairie, Minn. (1979).

61. American Society for Testing and Materials Standard #C373-56 (1956).

62. Dr. Noel Jarrett, (ALCOA), Personal Communication.

63. Joint Committee on Powder Diffraction Standards, PDF #23-457

64. R.H. Radzilowski and J.T. Kummer, Inorg. Chem., 8, p.2531 (1969).

65. M. Vardelle and J.L. Besson, Ceram. Int., 7, p.48 (1981).

66. JANAF Thermochemical Tables, Second Edition.

67. L. Brewer and A.W. Searcy, J.Am. Chem. Soc., 73, p.5313 (1951).

68. H. Yanagida and F.A. Kroger, J. Am. Ceram.Soc. 51, p.700 (1968).

69. J. Drowart, G. DeMaria, R.P. Burns and M.G. Inghram, J.of Chem. Phys., 32, p.1366 (1960).

70. R.F. Porter, P.Schissel and M.G. Inghram, J.Chem. Phys. 23, p.339 (1955).

71. P.O. Schissel and W.S.Williams, Bull. Am. Phys. Soc. II, 4, p.139 (1959).

72. W.L. Worrell, Can. Met. Quart., 4, P.87, (1965).

73. W.D. Kingery, H.K. Bowen, and D.R. Uhlmann, "Introduction to Ceramics, Second Edition," p. 402, John Wiley & Sons Inc, (1976).

74. G. Yamaguchi and T. Tokuda, Bull. of the Chem. Soc. of Japan, 80, p. 843 (1967).

75. H. Schmalzried, "Solid State Reactions," Chapter 6, Academic Press, New York, 1974.

76. F.S. Pettit, E.H. Randklev, and E.J. Felten, J. Am. Ceram. Soc., 49, p.199 (1966).

77. R.E. Carter, J. Am. Ceram. Soc., 44, p.116 (1961).

Biographical Note

Normand Corbin was born and grew up in Salem, Massachusetts. He was graduated in June 1978 from Northeastern University with a bachelor of science degree in geology. While attending Northeastern University he worked as a laboratory assistant in the Ceramics Division at the U.S. Army Materials and Mechanics Research Center (AMMRC) in Watertown, Mass. After graduation he stayed at AMMRC and attended M.I.T. as a special student. In September of 1981 Normand was sent by AMMRC to attend M.I.T. and conduct thesis work under the guidance of Prof. R.L. Coble on aluminum oxynitride materials.

He has coauthored reports on oxynitride ceramics, pyrophoric materials, and powder characterization.